



Contents lists available at SciVerse ScienceDirect



Ocean Modelling

journal homepage: www.elsevier.com/locate/ocemod

Level-ice melt ponds in the Los Alamos sea ice model, CICE

Elizabeth C. Hunke^{a,*}, David A. Hebert^b, Olivier Lecomte^c^a T-3 Fluid Dynamics and Solid Mechanics Group, Theoretical Division, Los Alamos National Laboratory, Los Alamos, New Mexico, USA^b Oceanography Division, Naval Research Laboratory, Stennis Space Center, Mississippi, USA^c Georges Lemaître Center for Earth and Climate Research, Earth and Life Institute, Université Catholique de Louvain, Louvain-la-Neuve, Belgium**ARTICLE INFO****Article history:**

Available online xxxx

Keywords:
 Sea ice
 Albedo
 Melt ponds
 Ridging
 Modeling
 Arctic

ABSTRACT

A new meltpond parameterization has been developed for the CICE sea ice model, taking advantage of the level ice tracer available in the model. The ponds evolve according to physically based process descriptions, assuming a depth-area ratio for changes in pond volume. A novel aspect of the new scheme is that the ponds are carried as tracers on the level ice area of each thickness category, thus limiting their spatial extent based on the simulated sea ice topography. This limiting is meant to approximate the horizontal drainage of melt water into depressions in ice floes. Simulated melt pond processes include collection of liquid melt water and rain into ponds, drainage through permeable sea ice or over the edges of floes, infiltration of snow by pond water, and refreezing of ponds. Furthermore, snow that falls on top of ponds whose top surface has refrozen blocks radiation from penetrating into the ponds and sea ice below.

Along with a control simulation, we present a range of sensitivity tests to parameters related to each subprocess described by the parameterization. With the exception of one parameter that alters the albedo of snow-covered pond ice, results are not highly sensitive to these parameters unless an entire process is removed. The snow simulation itself is critical, because the volume of snow deposition and rate of snow melt largely determine the timing and extent of the simulated melt ponds. Nevertheless, compensating effects moderate the model's sensitivity to precipitation changes. For instance, infiltration of the snow by melt water postpones the appearance of ponds and the subsequent acceleration of melting through albedo feedback, while snow on top of refrozen pond ice also reduces the ponds' effect on the radiation budget.

By construction, the model simulation of level and ridged ice is also important for this parameterization. We find that as sea ice thins, either through time or when comparing sensitivity tests, the area of level ice increases. This leads to an enhanced thinning feedback in the model, because a greater ice area may be exposed to ponding and further thinning due to lowered albedo.

© 2012 Elsevier Ltd. All rights reserved.

1. Introduction

Surface characteristics determine the surface energy balance of sea ice. Sea ice volume is highly sensitive to the thermodynamic fluxes that determine this balance, of which short- and longwave radiation are critical components in summer. Summer melt ponds, pools of melted snow and ice that collect in depressions on the ice surface, can lower the surface albedo considerably from the relatively high values associated with snow cover and bare ice (Perovich et al., 2002a; Grenfell and Perovich, 2004). The surface albedo continues to decrease as more melt water collects on the ice, increasing solar absorption and further melting the ice and snow, an important albedo feedback process (Curry et al., 1995; Perovich et al., 2003). The formation, evolution and disappearance

of melt ponds are governed by complex processes, including interactions with the existing snow layer, drainage rates through permeable sea ice, episodic refreezing and considerations of ice topography (Eicken et al., 2004; Polashenski et al., 2012), making detailed melt pond modeling a daunting task.

In this section we provide overviews of prior meltpond modeling work and our new parameterization. Detailed descriptions of the physical processes modeled in our scheme appear in Section 2, with the model configuration given in Section 3. Control run and sensitivity simulations are compared with available observational data in Section 4, considering the effects of parameters intrinsic to the scheme along with entire subprocesses and prescribed precipitation amount. Changes in average Arctic sea ice characteristics from the decade 1988–1997 to 1998–2007 are also explored in Section 4, with special attention to melt ponds. Several conclusions can be drawn from this interdecadal comparison, beyond the expected increase in ponding and sea ice thinning; these are discussed in Section 5. In particular, a feedback between the

* Corresponding author. Address: MS-B216, Los Alamos National Laboratory, Los Alamos, NM 87545, USA. Tel.: +1 505 665 9852; fax: +1 505 665 5926.

E-mail address: oclare@lanl.gov (E.C. Hunke).

fraction of level ice available and its propensity toward ponding and lower ice albedo may accelerate sea ice volume reduction.

1.1. Prior work

In the current release of the Los Alamos sea ice model (CICE version 4.1), there are two meltpond parameterizations available. In the original scheme, ponds are implicit, that is, their radiative effects are modeled through the albedo parameterization without explicitly accounting for meltpond physical processes such as the collection of melt water into pools. The albedo depends on the temperature and thickness of ice and snow and on the spectral distribution of the incoming solar radiation (Hunke, 2010). Parameters are chosen such that the average sea ice albedo behaves similarly to that observed when melt ponds would be present as well as throughout the rest of the year.

A newer, explicit meltpond parameterization is designed to be used in conjunction with the multiple-scattering radiation scheme available in CICE (Holland et al., 2012), and is employed for the most recent cycle of climate model projections in the Community Earth System Model (CESM, also known as the Community Climate System Model, CCSM4, Gent et al., 2011). Meltpond volume is carried on each ice thickness category as an area tracer and grows through addition of melt water from snow and ice or rain water, and shrinks when the ice surface temperature becomes cold. These processes are described empirically. Pond depth is assumed to be a linear function of the pond fraction and is limited by the category ice thickness.

Other meltpond parameterizations have been developed. Taylor and Feltham (2004) developed a one-dimensional sea ice model based on mushy-layer theory that includes ponds as a liquid phase along with a two-stream radiation scheme. Lüthje et al. (2006) modeled melt pond evolution using a cellular automaton that responds to horizontal fluxes in addition to vertical seepage of melt water through the ice, and thus can account for variations in topographical surface features. A very different kind of model was presented by Skillingstad et al. (2009), in which melt water flows freely through porous, level ice. The pond depth corresponds to local sea level, and sea ice topography is imposed based on direct observations or photographs. Scott and Feltham (2010) combined the approaches of Taylor and Feltham (2004) and Lüthje et al. (2006) to produce three dimensional simulations of melt pond evolution that included improved physical features such as snow topography and hydraulic meltwater transport rates both laterally and vertically.

Departing from the cellular automaton approach, Flocco and Feltham (2007) and Flocco et al. (2012) applied mathematical descriptions of physical melt pond processes to the CICE model, utilizing its ice thickness distribution to approximate the effects of topography on melt pond evolution. In their approach, melt water pools on the thinnest ice categories first, saturating remaining snow, with an imposed maximum fractional coverage that depends linearly on ice thickness as in Lüthje et al. (2006). Ponds drain vertically through sea ice when it is permeable, and refreeze when the surface energy balance is negative. In Flocco and Feltham (2007), the pond volume was carried as an ice area tracer, but in Flocco et al. (2012), pond area and thickness are carried as separate tracers, as in the meltpond parameterization described herein.

1.2. Overview of the level-ice meltpond scheme

We present a new meltpond parameterization that takes advantage of the level ice tracer available in the CICE model. The parameterization represents a combination of ideas from the CESM melt pond scheme (Holland et al., 2012), also available in CICE, and that of Flocco et al. (2010, 2012). In particular, we kept the underlying

assumption of pond shape from the CESM scheme, but only for changes in pond volume – not for the ponds themselves. In CESM, pond depth is given by $h_p = \delta_p a_p$, where $\delta_p = 0.8$ and a_p is the fraction of ice covered by ponds. We use a similar formulation for changes in pond volume, $\Delta h_p = \delta_p \Delta a_p$. We replace the empirical formulas that CESM uses with their physically based counterparts, similarly to Flocco et al. (2010, 2012).

The novel aspect of our melt pond scheme is that the ponds are carried as tracers only on the simulated level ice area. This is a similar concept to that of Flocco et al. (2010, 2012), but more refined in scale. In their case, melt water is moved from thicker ice categories and collected on the thinnest categories. In our case, the water is moved from the deformed ice area within each category, onto the undeformed (level) ice in the same category. The shape of the pond develops over time based on the assumed aspect ratio δ_p of changes in pond volume along with horizontal transport and other sea ice physical processes. Thus the pond area may cover only a small portion of the level ice area.

Melt pond processes, described in more detail below, include addition of liquid water from rain, melting snow and melting surface ice, drainage of pond water over the sides of floes or when the ice interior becomes permeable, and refreezing of the pond water. If snow falls after a layer of ice has formed on the ponds, the snow may block sunlight from reaching the ponds below. These processes have been included in prior models (e.g., Flocco et al., 2010, 2012). The following snow and radiative processes have not been included in pond parameterizations before, or are modeled here in a different manner from prior work.

When meltwater forms with snow still on the ice, the water is assumed to infiltrate the snow. If there is enough water to fill the air spaces within the snowpack, then the pond becomes visible above the snow, thus decreasing the albedo and ultimately causing the snow to melt faster. The albedo also decreases as snow depth decreases, and thus a thin layer of snow remaining above a pond-saturated layer of snow will have a lower albedo than if the melt water were not present.

Radiatively, the surface of an ice category is divided into fractions of snow, pond and bare ice. The presence of a refrozen ice lid on top of a pond does not affect the radiation reaching the pond below unless there is snow on top of the pond ice, in which case the surface type of the pond fraction is considered to be snow rather than liquid water. If the pond ice is melting, the shortwave flux used to melt it is blocked from entering the pond below. These processes do not alter the actual pond volume; instead they are used to define an “effective pond fraction” (and likewise, effective pond depth, snow fraction and snow depth) used only for the shortwave radiation calculation.

1.3. Tracers

The basic conservation equations for ice area fraction a_i , level ice fraction $a_{lvi}a_i$, pond area fraction $a_{pnd}a_{lvi}a_i$, pond volume $h_{pnd}a_{pnd}a_{lvi}a_i$ and pond ice volume $h_{ipnd}a_{pnd}a_{lvi}a_i$, given the ice velocity \mathbf{u} , are

$$\frac{\partial}{\partial t}(a_i) + \nabla \cdot (a_i \mathbf{u}) = \frac{\Delta(a_i^+ + a_i^-)}{\Delta t} + \Psi, \quad (1)$$

$$\frac{\partial}{\partial t}(a_{lvi}a_i) + \nabla \cdot (a_{lvi}a_i \mathbf{u}) = \frac{\Delta(a_i^+ + a_{lvi}a_i^-)}{\Delta t} + \Psi_{lvi}, \quad (2)$$

$$\frac{\partial}{\partial t}(a_{pnd}a_{lvi}a_i) + \nabla \cdot (a_{pnd}a_{lvi}a_i \mathbf{u}) = \frac{1}{\delta_p} \sqrt{\frac{\Delta V}{\Delta t}}, \quad (3)$$

$$\frac{\partial}{\partial t}(h_{pnd}a_{pnd}a_{lvi}a_i) + \nabla \cdot (h_{pnd}a_{pnd}a_{lvi}a_i \mathbf{u}) = \frac{\Delta V}{\Delta t}, \quad (4)$$

$$\frac{\partial}{\partial t}(h_{ipnd}a_{pnd}a_{lvl}a_i) + \nabla \cdot (h_{ipnd}a_{pnd}a_{lvl}a_i \mathbf{u}) = -\frac{\rho_0}{\rho_i} \frac{\Delta V_{ipnd}}{\Delta t}. \quad (5)$$

The forcing terms on the right hand sides of these equations represent sources and sinks and are written here in discrete form for convenient comparison with their descriptions in Section 2. In Eq. (1), Δa_i^+ and Δa_i^- represent new ice growth and lateral melting, respectively, and Ψ represents ice deformation processes (ridging, rafting). The same processes are included in Eq. (2), although in different proportions. For instance, all new ice growth is level ice, but lateral melting affects both level and deformed ice in Eq. (1) and only level ice in Eq. (2); only the area of level ice destroyed by deformation is included in Ψ_{lvl} . $\Delta V = \Delta V_{melt} + \Delta V_{perm} + \Delta V_{iso} + \Delta V_{ipnd}$ includes accumulation of rain, snow and ice melt (ΔV_{melt}) along with pond drainage associated with permeability (ΔV_{perm}) and isostatic adjustment (ΔV_{iso}), and phase changes associated with pond ice (ΔV_{ipnd}). Refrozen pond ice volume (Eq. (5)) is governed by new growth and melting at the top of ponds, ΔV_{ipnd} , adjusted for density differences using ρ_0 and ρ_i , the densities of fresh water and ice, respectively.

These pond sources and sinks are described in more detail in Section 2; for a complete description of other sea ice processes parameterized in CICE, see Hunke and Lipscomb (2010). The advection terms in Eqs. (1)–(5) are solved using an incremental remapping algorithm (Lipscomb and Hunke, 2004), with thermodynamic forcing terms obtained using the Bitz and Lipscomb (1999) thermodynamic model. The thickness distribution (Thorndike et al., 1975) employs 5 ice thickness categories, and mechanical deformation is based on the energetics-based approach of Rothrock (1975). Sea ice velocity and deformation rates are obtained using the elastic–viscous–plastic dynamics formulation (Hunke and Dukowicz, 1997, 2002; Hunke, 2001).

Eqs. (4) and (5) express conservation of melt pond volume and pond ice volume, but in this form highlight that the quantities tracked in the code are the tracers h_{pnd} and h_{ipnd} , pond depth and pond ice thickness. Likewise, the level ice fraction a_{lvl} is a tracer on ice area fraction (Eq. (2)), and pond fraction a_{pnd} is a tracer on level ice (Eq. (3)).

For a generic quantity q that represents a mean value over the ice fraction, qa_i is the average value over the grid cell. Thus h_{pnd} can be considered the actual pond depth, $h_{pnd}a_{pnd}$ is the mean pond depth over the level ice, $h_{pnd}a_{pnd}a_{lvl}$ is the mean pond depth over the sea ice, and $h_{pnd}a_{pnd}a_{lvl}a_i$ is the mean pond depth over the grid cell. Here, for brevity, we denote $a_p = a_{pnd}a_{lvl}$, the ponded fraction of the sea ice. Throughout this paper, equations represent quantities within one thickness category; all melt pond calculations are performed separately for each category.

2. Meltpond processes

2.1. Melt water

Liquid water may be produced on a given category by melting snow and the surface of the ice, and may be supplemented with the addition of liquid precipitation. Some of this volume may run off into the ocean, and the remainder, ΔV_{melt} , is added to the melt pond liquid volume:

$$\Delta V_{melt} = r(\rho_i|\Delta h_i| + \rho_s|\Delta h_s| + F_{rain}\Delta t)a_i,$$

where

$$r = r_{min} + (1 - r_{min})a_i \quad (6)$$

is the fraction of the total melt water available that is added to the ponds, ρ_i and ρ_s are ice and snow densities, $|\Delta h_i|$ and $|\Delta h_s|$ are the thicknesses of ice and snow that melted, and F_{rain} is the rainfall rate.

The parameter r_{min} is the minimum volume fraction of melt water that remains on the ice for small ice area fraction (as $a_i \rightarrow 0$).

2.2. Pond ice

The ponds are assumed to consist of well-mixed, fresh water, and therefore their temperature is 0 °C. If the air temperature is cold enough, a layer of clear ice may form on top of the ponds. In CICE, we track the thickness of the ice lid using the tracer h_{ipnd} and include the radiative effect of snow on top of the lid.

We use a Stefan approximation for growth of fresh ice, invoked only when $\Delta V_{melt} = 0$. The basic thermodynamic equation governing ice growth is

$$\rho_i L \frac{\partial h_i}{\partial t} = k_i \frac{\partial T_i}{\partial z} \sim k_i \frac{\Delta T}{h_i} \quad (7)$$

assuming a linear temperature profile (slope ΔT) through the ice thickness h_i . The ice conductivity k_i is a function of salinity following Pringle et al. (2007). Defining a parameter β ,

$$\beta = \frac{2k_i\Delta T}{\rho_i L},$$

Eq. (7) becomes

$$\frac{\partial h_i}{\partial t} = \frac{1}{2} \sqrt{\frac{\beta}{t}} = \frac{\beta}{2h_i}. \quad (8)$$

with $h_i(t) = \sqrt{\beta t}$. In discrete form we have

$$\Delta h_i = \begin{cases} \sqrt{\beta \Delta t}/2 & \text{if } h_i = 0, \\ \beta \Delta t/2h_i & \text{if } h_i > 0. \end{cases} \quad (9)$$

When $\Delta V_{melt} > 0$, any existing pond ice may also melt. In this case,

$$\Delta h_i = -\min\left(\frac{\max(F_o, 0)\Delta t}{\rho_i L}, h_i\right), \quad (10)$$

where F_o is the net downward surface flux.

In either case, the change in pond volume associated with growth or melt of pond ice is

$$\Delta V_{ipnd} = -\Delta h_i a_{pnd} a_{lvl} a_i \rho_i / \rho_0,$$

where ρ_0 is the density of fresh water.

2.3. Drainage

A portion $1 - r$ of the available melt water drains immediately into the ocean. Once the volume changes described above have been applied and the resulting pond area and depth calculated, the pond depth may be further reduced if the top surface of the ice would be below sea level or if the sea ice becomes permeable.

2.3.1. Negative freeboard

We require that the sea ice surface remain at or above sea level. If the weight of the pond water would push the mean ice–snow interface of a thickness category below sea level, some or all of the pond water is removed to bring the interface back to sea level. That is, we utilize Archimedes' Principle written in terms of the draft d ,

$$\rho_i h_i + \rho_s h_s + \rho_0 h_p = \rho_w d \leq \rho_w h_i,$$

to determine an isostatic volume adjustment when $d > h_i$,

$$\Delta V_{iso} = (h_i - d)a_{pnd}a_{lvl}a_i \leq 0.$$

There is a separate freeboard calculation which considers only the ice and snow, and converts flooded snow to sea ice. Because the current melt ponds are “virtual” in the sense that they only

have a radiative influence, we do not allow the pond mass to change the sea ice and snow masses at this time, although this issue may need to be reconsidered in the future, especially for the Antarctic.

2.3.2. Permeability

Sea ice permeability is calculated using the internal ice temperatures T_i (computed from the enthalpies as in the sea ice thermodynamics). The brine salinity and liquid fraction are given by (Notz, 2005, Eq. (3.6)) $S_{br} = (10^{-3} - 0.054/T_i)^{-1}$ and $\phi = S/S_{br}$, where S is the bulk salinity of the combined ice and brine. The ice is considered permeable if $\phi \geq 0.05$, with a permeability of $p = 3 \times 10^{-8} \text{ min}(\phi)$, the minimum being taken over all of the ice layers.

A pressure head is computed as $P = g\rho_w\Delta h$ where Δh is the height of the pond and sea ice above sea level. Then the volume drained from the pond is given by

$$\Delta V_{perm} = -a_i d_p \min\left(h_{pnd}, \frac{pP\Delta t}{\mu h_i}\right),$$

where d_p is a scaling factor, and $\mu = 1.79 \times 10^{-3} \text{ kg m}^{-1} \text{ s}^{-1}$ is the dynamic viscosity.

2.4. Ridging and new ice formation

There are two more cases in which the tracers need to be modified for physical reasons, namely when ice ridges and when new ice forms in open water. Both cases affect the level ice area, and ponds must be handled appropriately. For example, when sea ice deforms, some of the level ice is transformed into ridged ice. We assume that pond water (and pond ice) on the portion of level ice that ridges is lost to the ocean.

When new ice forms in open water, level ice is added to the existing sea ice, but the new level ice does not yet have ponds on top of it. Therefore the fractional coverage of ponds on level ice decreases (thicknesses are unchanged). This is accomplished by maintaining the same mean pond area in a grid cell after the addition of new ice,

$$a'_{pnd}(a_{lvl} + \Delta a_i)(a_i + \Delta a_i) = a_{pnd}a_{lvl}a_i,$$

and solving for the new pond area tracer a'_{pnd} given the newly formed ice area Δa_i .

2.5. The shape of volume changes

In this melt pond scheme, the actual pond area and depth are maintained separately throughout the simulation according to the physical processes acting on it. This is different from the CESM melt pond scheme, in which the pond volume is maintained; in that case the area and depth are computed according to the assumed pond shape. Here, pond volume changes are distributed as changes to the area and to the depth of the ponds using an assumed aspect ratio, or shape, given by the parameter δ_p , where $\delta_p = \Delta h_p/\Delta a_p$ and $\Delta V = \Delta h_p \Delta a_p = \delta_p \Delta a_p^2 = \Delta h_p^2/\delta_p$. Here, $a_p = a_{pnd}a_{lvl}$, the mean pond area over the ice, following CESM. The value $\delta_p = 0.8$ used in CESM and here was derived by fitting a line to observed SHEBA data (Holland et al., 2012).

Finally, if a quantity such as a_i or a_{lvl} becomes zero in a grid cell's thickness category, then all tracers that depend on it also become zero.

2.6. Snow infiltration by pond water

Snow on the sea ice and pond ice may shield the pond and ice below from solar radiation, and therefore "effective" pond area

and depth are computed for use during the radiation calculation. For instance, when there is snow on top of the sea ice, melt water may infiltrate the snow. The snow infiltration parameterization does not directly affect the thermodynamics of the model in the sense that it does not make the snow melt and does not affect the snow heat content. It is a "virtual process" that affects the model's thermodynamic calculation through the input parameters of the radiation scheme.

Consider the amount of retained melt water V_p compared to the Snow Water Equivalent (SWE) given by $SWE = V_s \rho_s / \rho_0$, where ρ_s , ρ_0 and V_s are the densities of snow and fresh water and the volume (per unit area) of snow, respectively. The volume fraction of retained melt water to total liquid content is

$$r_p = \frac{V_p}{V_p + SWE}.$$

A snow pack is considered saturated when its percentage of liquid water content is greater or equal to 15% (Jordan et al., 2008; Sturm and Massom, 2010), and we assume that if $r_p < 0.15$ then effectively there are no meltponds present, that is, $a'_{pnd} = h'_{pnd} = 0$. Otherwise, we assume that the snowpack is saturated with liquid water.

Liquid water percolates down very quickly into the snow. Here we assume that all of the liquid water accumulates at the base of the snow pack and would eventually melt the surrounding snow. Two configurations are therefore possible, (1) the top of the liquid ponds lies below the snow surface and (2) the liquid water volume overtops the snow, and all of the snow is assumed to have melted into the pond. The volume of void space within the snow that can be filled with liquid melt water is

$$V_{mx} = h_{mx} a_p = \left(\frac{\rho_0 - \rho_s}{\rho_0} \right) h_s a_p,$$

and we compare V_p with V_{mx} .

Case 1: for $V_p < V_{mx}$, we define V_p^{eff} to be the volume of void space filled by the volume V_p of melt water:

$$\rho_0 V_p = (\rho_0 - \rho_s) V_p^{eff}$$

or in terms of depths,

$$h_p^{eff} = \left(\frac{\rho_0}{\rho_0 - \rho_s} \right) h_{pnd}.$$

The liquid water under the snow layer is not visible and therefore the ponds themselves have no direct impact on the radiation ($a_{pnd}^{eff} = h_{pnd}^{eff} = 0$), but the effective snow thickness used for the radiation scheme is reduced to

$$h_s^{eff} = h_s - h_p^{eff} a_p = h_s - \frac{\rho_0}{\rho_0 - \rho_s} h_{pnd} a_p.$$

Here, the factor $a_p = a_{pnd}a_{lvl}$ averages the reduced snow depth over the ponds with the full snow depth over the remainder of the ice; that is, $h_s^{eff} = h_s(1 - a_p) + (h_s - h_p^{eff})a_p$.

Case 2: similarly, for $V_p \geq V_{mx}$, the total mass in the liquid is

$$\rho_0 V_p + \rho_s V_s = \rho_0 V_p^{eff}$$

or

$$h_p^{eff} = \frac{\rho_0 h_{pnd} + \rho_s h_s}{\rho_0}.$$

Thus the effective depth of the pond is the depth of the whole slush layer h_p^{eff} . In this case, $a_{pnd}^{eff} = a_{pnd}a_{lvl}$.

2.7. Snow atop pond ice

Freshwater ice that has formed on top of a melt pond is assumed to be perfectly clear. Snow may accumulate on top of the

pond ice, however, shading the pond and ice below. The depth of the snow on the pond ice is initialized as $h_{ps}^0 = F_{snow}\Delta t$ at the first snowfall after the pond ice forms. From that time until either the pond ice or the pond snow disappears, the pond snow depth tracks the depth of snow on sea ice (h_s) using a constant difference Δ such that $h_s - h_{ps} = \Delta$. Thus for example, as new snow falls both h_s and h_{ps} increase at the same rate. As h_s melts, $h_{ps} = h_s - \Delta$ will be reduced to zero eventually, at which time the pond ice is fully uncovered and shortwave radiation passes through unhindered.

To prevent a sudden change in the shortwave reaching the sea ice (which can prevent the thermodynamics solver from converging), thin layers of snow on pond ice are assumed to be patchy, thus allowing the shortwave flux to increase gradually as the layer thins. This is done using the same parameterization for patchy snow as is used elsewhere in CICE, but with its own parameter h_{s1} :

$$a_{pnd}^{eff} = \left(1 - \min\left(\frac{h_{ps}}{h_{s1}}, 1\right)\right) a_{pnd} a_{lvl}.$$

If any of the pond ice melts, the radiative flux allowed to pass through the ice should be reduced by the flux required to melt that ice. This is accomplished approximately with $a_{pnd}^{eff} = (1 - f_{frac}) a_{pnd} a_{lvl}$, where (see Eq. (10))

$$f_{frac} = \min\left(-\frac{\rho_i L \Delta h_i}{F_o \Delta t}, 1\right).$$

2.8. Differences with Flocco et al.

Although we have not yet attempted to compare our results with those of Flocco et al. (2010, 2012), whose parameterization also is implemented in CICE, the two schemes share a number of common elements with subtle differences that we want to distinguish in this description. The primary difference between the melt pond parameterization described above and that of Flocco et al. (2010, 2012) rests in the handling of melt water with respect to the ice thickness distribution. In particular, melt water accumulates in their scheme on the thinnest ice categories first, gradually covering thicker categories until the total melt water volume is distributed. In Flocco et al. (2010), 20% of the total melt water volume initially ran off the ice, but in Flocco et al. (2012) a formula similar to Eq. (6) is used, $r = 0.15 + 0.7a$. Each category may be covered up to the fraction $0.832 - 0.24h_i$ in their scheme, so that thicker ice categories carry a smaller ponded fraction than thinner categories. Likewise, thicker ice tends to be more highly deformed, thus limiting the pond area in our scheme.

As in the present parameterization, Flocco et al.'s melt water infiltrates the air spaces within the snow volume, but snow does not shadow their pond unless a refrozen ice lid thicker than 0.01 m is present on the pond. In that case, they ignore the pond's presence and assume the full snow depth covers the ice, unlike our parameterization in which only snow that has fallen since the ice lid formed lies on top of it. Both schemes apply a Stefan condition for the growth of pond ice, but with slightly different freezing temperatures (-0.15°C in theirs, 0°C in ours) and different numerical approximations. Regarding pond drainage, negative freeboard is not a consideration in their scheme because the ice thickness distribution within each grid cell is treated as a single, rigid ice floe whose thinnest categories may be below sea level. Our permeability formulae are the same with the exception of brine salinity (they use a combination of formulae from Notz (2005, Eq. (3.2)) and Assur (1958)), and they do not include the scaling factor d_p .

3. Model configuration

For the simulations described below, we configure the Los Alamos sea ice model, CICE, as in Hunke (2010), except for the parameterizations used for meltponds and shortwave absorption in the snow and ice column. In Hunke (2010), the albedo is parameterized in terms of the ice thickness, surface temperature and presence of snow in such a way that the radiative effects of melt ponds are incorporated implicitly. Here, we use the delta-Eddington radiation parameterization (Briegleb and Light, 2007; Holland et al., 2012) that requires an explicit melt pond parameterization, taking their depth and area fraction into account when computing radiative transfer through the ice. As in Hunke (2010), our simulations are forced with a combination of climatological ocean model output (12 months of surface salinity and slope, currents, and deep heat flux convergence), taken from the CCSM3 1990 control run b30.009 (Collins et al., 2006) and averaged over 20 years into an annual climatology of monthly values; radiation fields as specified by the Arctic Ocean Model Intercomparison Project (Hunke and Holland, 2007); and a modified version of the Common Ocean Reference Experiments (CORE, Griffies et al., 2009) atmospheric forcing fields for wind components, 10-m air temperature, humidity (all 6-hourly) and monthly climatological precipitation. One of our sensitivity runs uses CORE 6-hourly, interannually varying precipitation instead of the climatological field.

Two simulations were run to test sensitivity to initial conditions, a 50-year model simulation (1958–2007) identical to the 'ocnheat' run in Hunke (2010) except for the ponds and delta-Eddington radiation scheme, and a second run using the same model configuration as in the 50-year run, but starting from the 1 January 1980 sea ice state produced by the 'ocnheat' simulation in Hunke (2010) and run for 28 years, through 2007. After the first few years, the 1980–2007 simulation is not significantly different from the 50-year run, and therefore all of the simulations presented in this paper are initialized with the 1 January 1980 sea ice state from the new 50-year simulation; we analyze the two decades 1988–1997 and 1998–2007.

Table 1
Parameter values defining the control and sensitivity simulations.

Label	δ_p	r_{min}	d_p	Infiltration	r_{sat}	h_{s1}	h_{s0}	Description
CNTL	0.8	0.15	10^{-3}	T	0.15	0.03	0	Control run
TALL	[1.2]	0.15	10^{-3}	T	0.15	0.03	0	Taller ponds
FLAT	[0.4]	0.15	10^{-3}	T	0.15	0.03	0	Flatter ponds
RFFUP	0.8	[0.0]	10^{-3}	T	0.15	0.03	0	More runoff
RFFDN	0.8	[1.0]	10^{-3}	T	0.15	0.03	0	No runoff
PERM	0.8	0.15	[0.0]	T	0.15	0.03	0	No permeable drainage
INFL	0.8	0.15	10^{-3}	[F]	–	0.03	0	No snow infiltration
RPO	0.8	0.15	10^{-3}	T	[0.0]	0.03	0	Lower saturation minimum
RP03	0.8	0.15	10^{-3}	T	[0.3]	0.03	0	Higher saturation minimum
HS1	0.8	0.15	10^{-3}	T	0.15	[0.1]	0	Patchy lid snow, $h_s \leq 0.1\text{ m}$
HS01	0.8	0.15	10^{-3}	T	0.15	[0.01]	0	Patchy lid snow, $h_s \leq 0.01\text{ m}$
PCIP	0.8	0.15	10^{-3}	T	0.15	0.03	0	Interannual precip data
CESM	0.8	0.15	–	–	–	–	0.03	CESM pond scheme

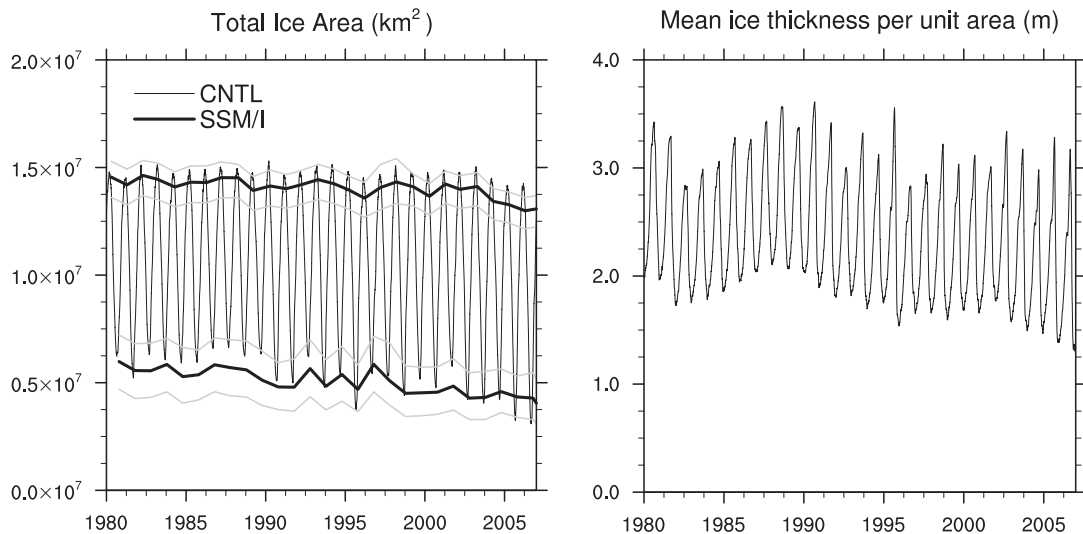


Fig. 1. Time series of Arctic ice area and mean thickness from CNTL. The gray lines indicate $\pm 5\%$ and $\pm 15\%$ ice concentration error estimates for the SSM/I data, in winter and summer respectively (Cavalieri et al., 1996, updated 2008).

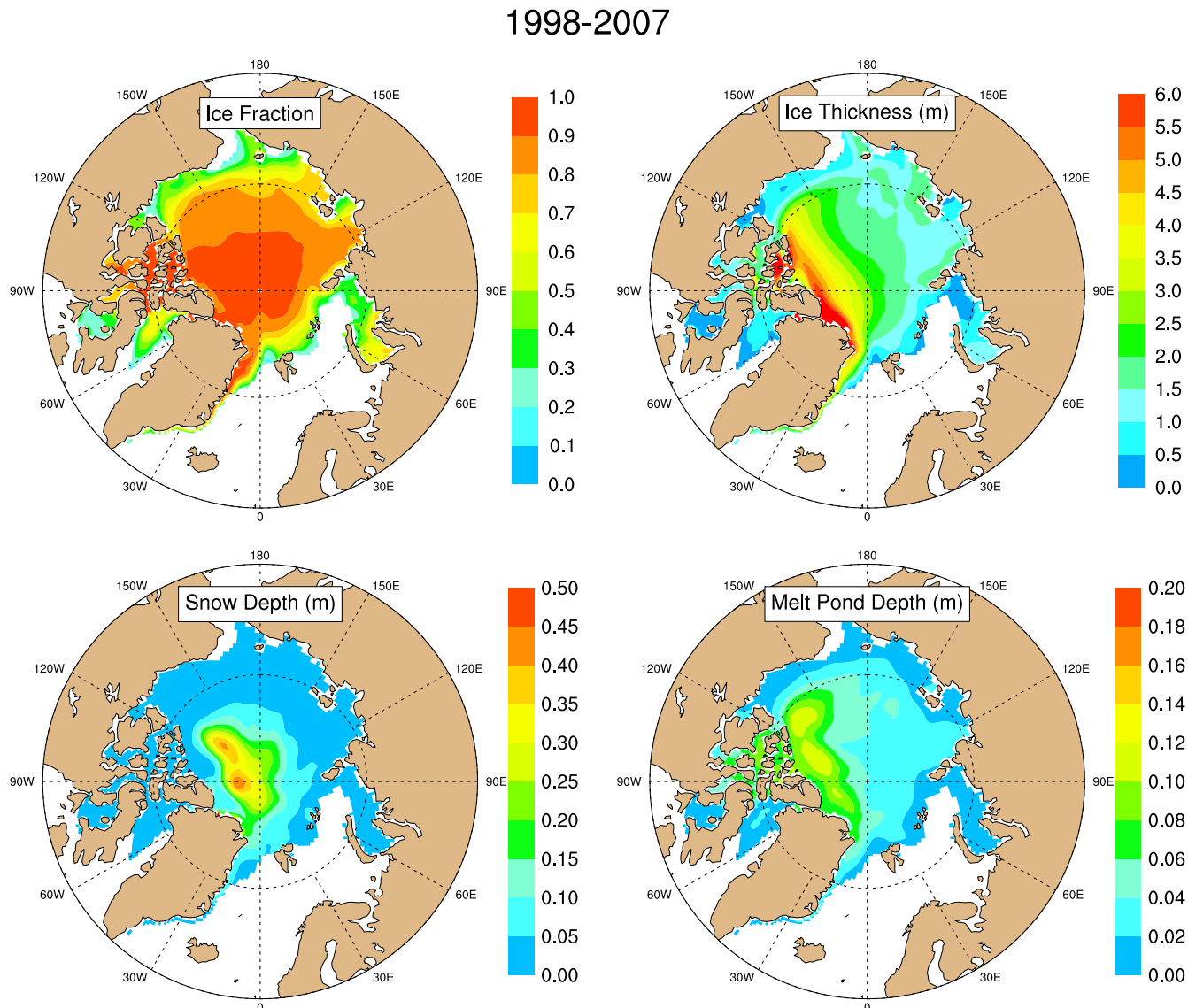


Fig. 2. July 1998–2007 mean ice area fraction, thickness, snow depth and pond depth from the CNTL simulation.

Table 1 provides an overview of the control run and sensitivity simulations, described in detail in the next section.

4. Simulation results

4.1. Control simulation

The control simulation “CNTL” uses a standard, but not necessarily optimal, set of parameters for the melt pond parameterization, as shown in **Table 1**. In particular, following CESM (Holland et al., 2012), we set the aspect ratio of pond depth to area $\delta_p = 0.8$ for pond volume changes, and the minimum volume fraction of retained melt water to $r_{min} = 0.15$. Likewise, we set the snow-on-pond-ice “patchiness” parameter $h_{s1} = 0.03$ in analogy with the CESM snow-on-sea-ice parameter h_{s0} . The scaling factor d_p for ice draining through permeable ice is given an order of

magnitude that corresponds to a 1-day e-folding time scale for pond drainage through 1-m thick ice. For the snow infiltration description, melt ponds do not appear until the snow pack is saturated, with $r_p \geq r_{sat} = 0.15$.

In the Arctic, both ice area and mean thickness show a decreasing trend since about 1988 that is most apparent in the summer minima, shown in **Fig. 1**. Total area in winter and summer are generally slightly larger than the SSM/I ice concentrations derived from brightness temperature, but within the range of uncertainty (Cavalieri et al., 1996, updated 2008). We filled the region of missing data surrounding the North Pole with 100% ice concentration.

Mean area fraction, thickness, snow depth and pond depth for July 1998–2007 are presented in **Fig. 2**. Spatial patterns of ice area and thickness are similar to the ‘ocnheat’ run from Hunke (2010). Replacing the default shortwave scheme used in the ‘ocnheat’ simulation (in which meltponds are accounted for implicitly) with the

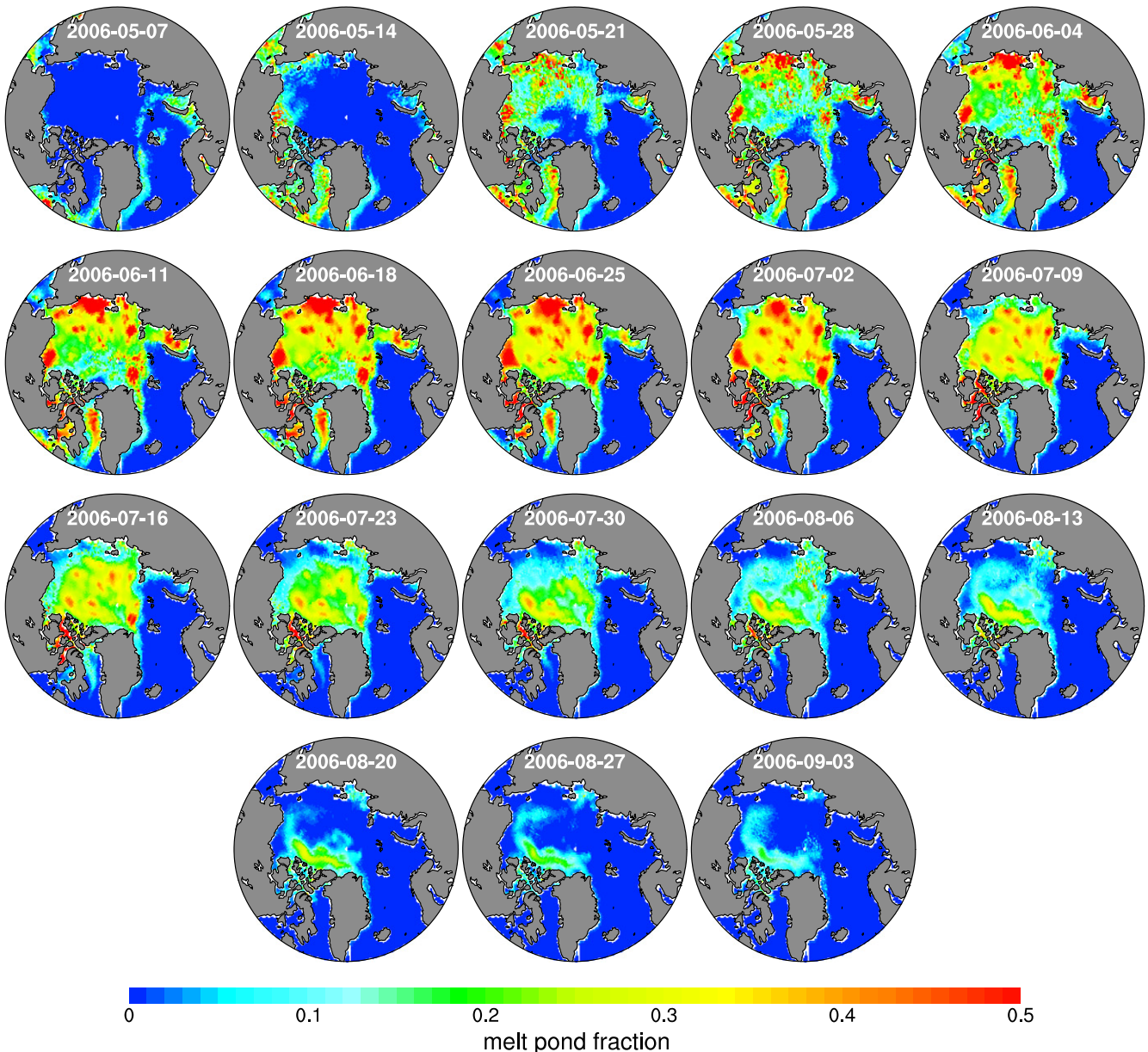


Fig. 3. Ponded fraction of ice area, in 2006, from the CNTL simulation.

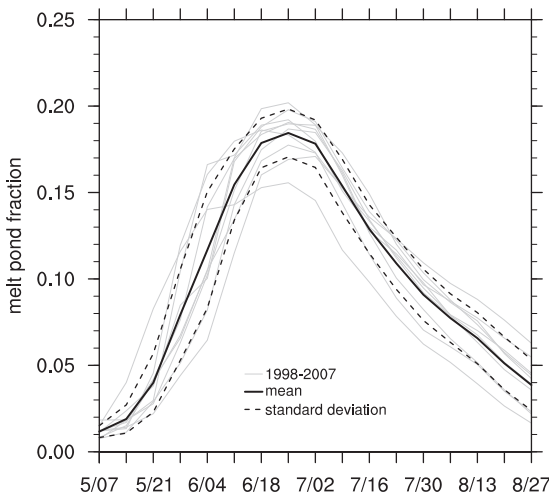


Fig. 4. Ponded fraction of grid cell area averaged over all ocean cells north of 60°N, from the CNTL simulation. The light lines show values for each year, 1998–2007.

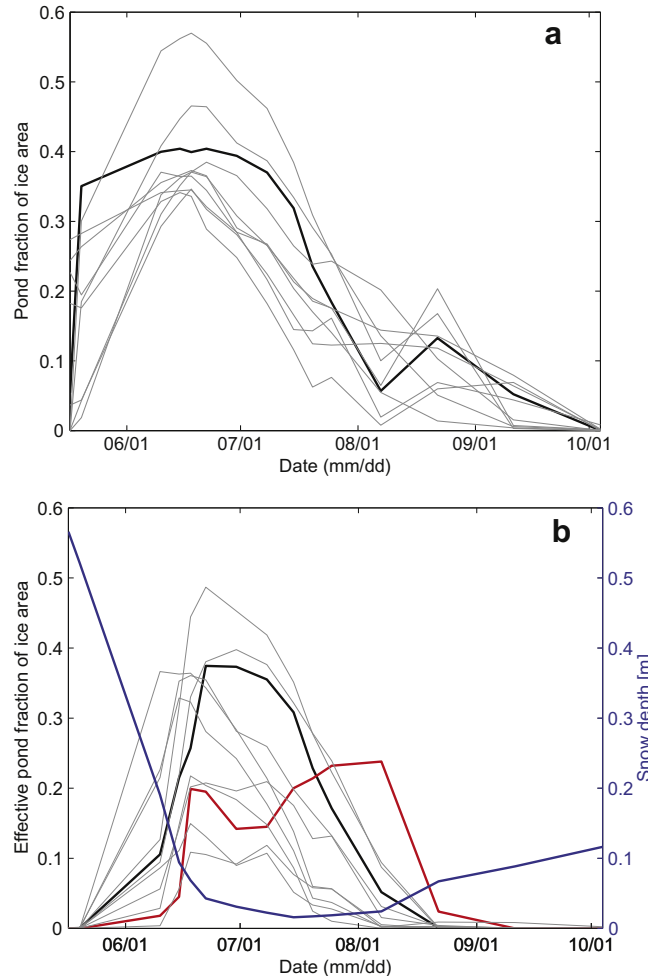


Fig. 5. CNTL (a) pond area and (b) effective pond area, given as a fraction of the ice area, for comparison with SHEBA data (red). The bold black line is model output for 1998; the thinner lines are 1999–2007. The blue line in (b) is the 1998 snow depth (right axis).

delta-Eddington radiation parameterization and the level-ice melt pond scheme thins the ice by approximately 0.11 m in the Arctic, on average through the year. We have not attempted to tune other

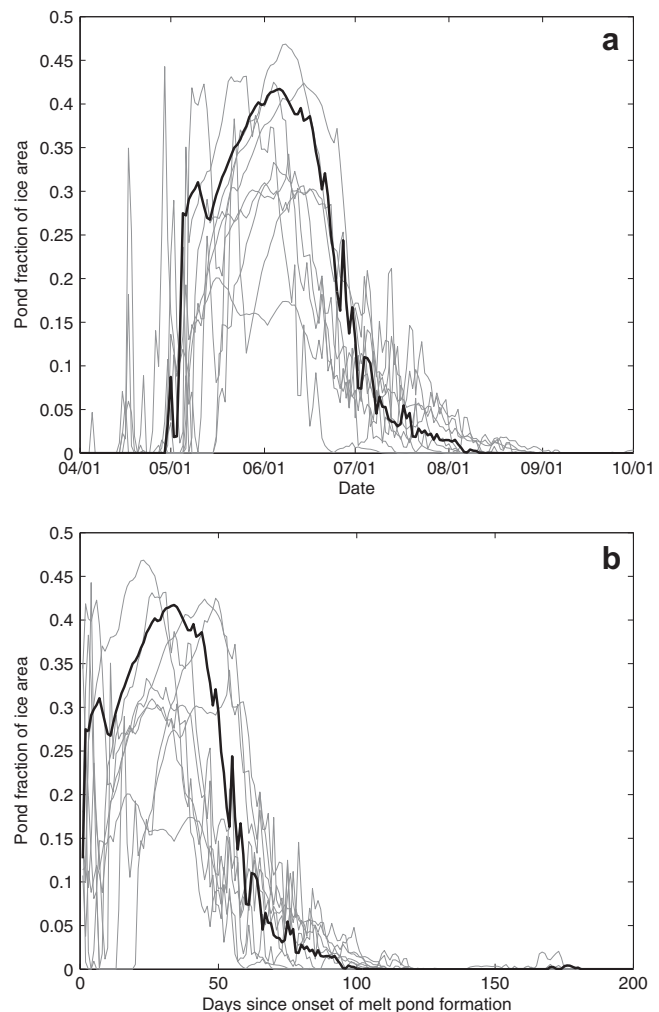


Fig. 6. Ponded fraction of ice area, at the grid cell nearest Barrow AK, plotted versus (a) date and (b) days since pond formation, from the CNTL simulation. For (b), “pond formation” occurs when the pond fraction first exceeds 0.1. The bold line is model output for 1998; the thinner lines are 1999–2007.

parameters to adjust the sea ice thickness produced in these simulations, as were discussed in Hunke (2010). Snow does not melt completely in the control simulation and thus hides a portion of the total melt pond water throughout the melt season. The deepest ponds form on the thickest ice, near Greenland and the Canadian Arctic. A larger fraction of this thicker sea ice is ridged, less level ice is available for ponding, and therefore melt water forms deeper pools (level ice characteristics are discussed further in Section 4.2). Melt ponds on rough, multiyear ice are observed to have lower areal coverage than on smoother ice types, due to deformation features and deepened melt pools on the rougher ice (Eicken et al., 2004; Polashenski et al., 2012).

Fig. 3 shows a weekly time series of 1-day average melt pond fraction of ice area for the whole Arctic, following Rösel et al. (2012). Ponds begin to appear at lower latitudes and spread northward. The largest fractional coverage remains near the periphery of the pack until after the maximum in late June. At that point, ponds nearer the ice edge drain (also, the sea ice itself melts away), leaving ponds only on thicker, less permeable ice (compare Fig. 2). These remaining ponds take longer to refreeze because they are comparatively deep. However, by later in the season, a lid of refrozen ice has formed on top of these ponds, covered in a layer of snow that effectively hides them.

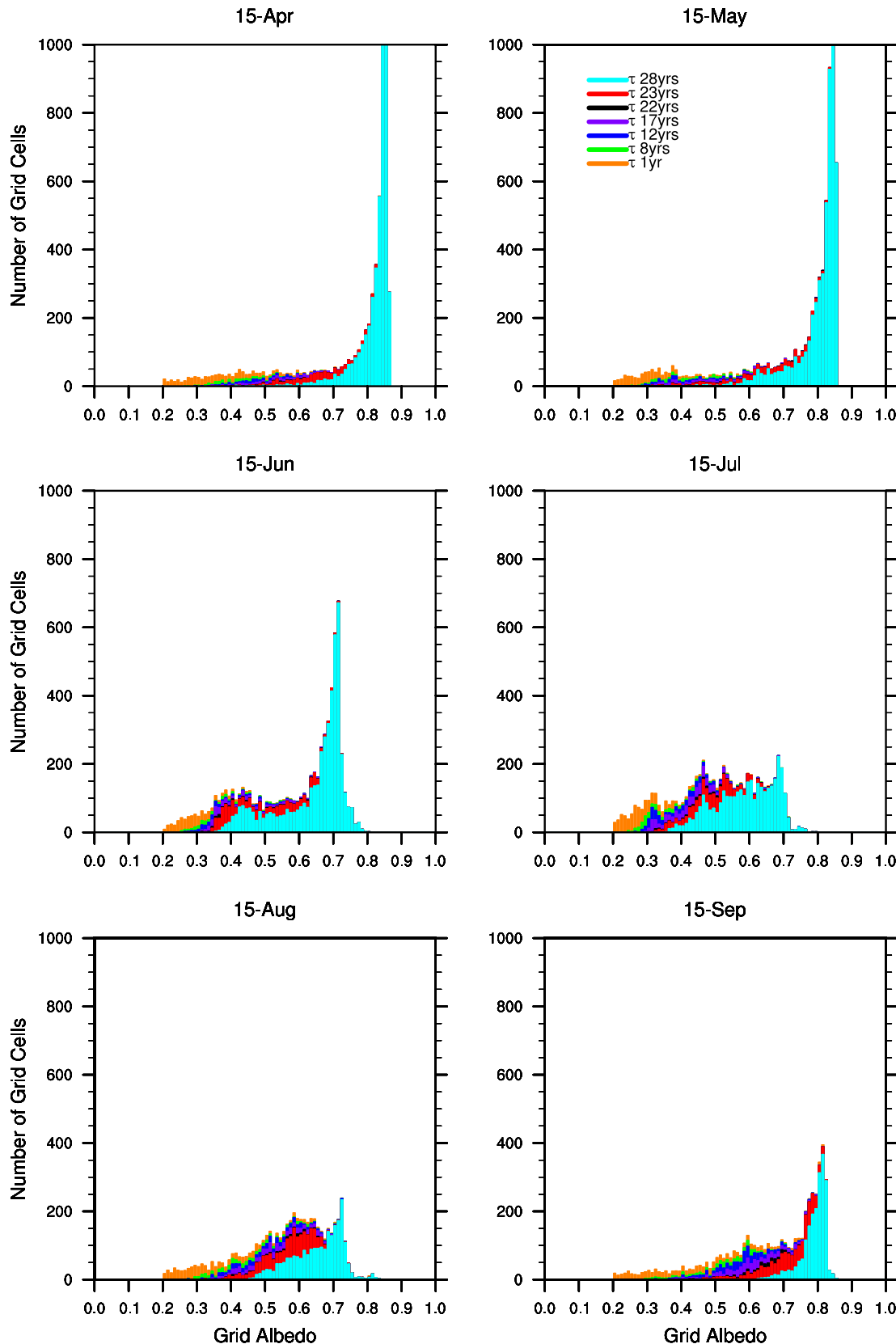


Fig. 7. Mean daily histograms of CNTL broadband surface albedo for all northern hemisphere grid cells, weighted for ocean fraction using the value 0.06 and plotted for the 15th of each month. Maximum grid cell count is 2515 for 15 April, 1508 for 15 May. The colors indicate the total number of cells containing sea ice for the duration shown in the legend, or longer, at any time during the simulation.

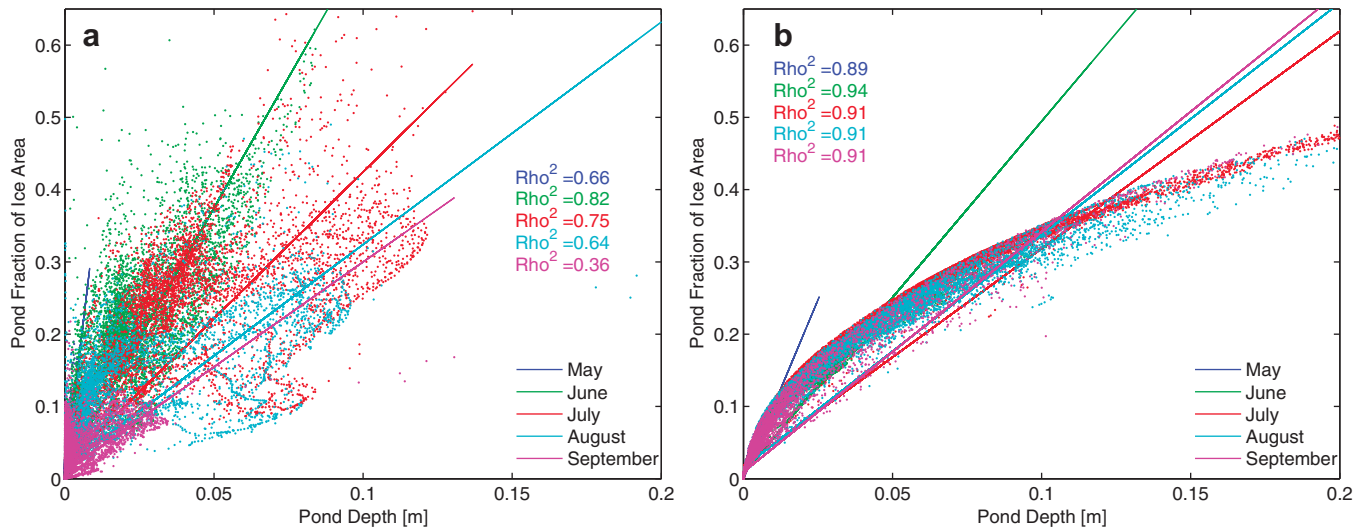


Fig. 8. Simulated pond fraction versus depth for (a) CNTL (b) CESM. The lines show a least-squares linear interpolant for each month. Rho^2 quantifies the fraction of variance explained by the least-squares fit.

The annual cycle of simulated melt pond fraction for the years 1998–2007 is shown in Fig. 4, for comparison with satellite-based estimates of Rösel et al. (2012). Our melt ponds are slower to appear above the snow in the spring, but they reach maximum coverage at the same time as in the observations, in this hemispheric average. Rösel et al.'s data show 0.9 on 18 May and 24 August, and a maximum of about 0.15 around 25 June.

The effect of the spring snow cover is apparent in Fig. 5, which shows the modeled, actual pond area and the radiatively effective pond area as a fraction of the ice area for the model grid cells and times corresponding to the SHEBA field experiment in 1998 (Perovich et al., 2002b). Snow does not disappear entirely in the simulation, hence there is some reduction in effective pond area due to snow throughout the melt season. However, the largest effects occur during spring and fall. In May and early June, melt ponds shallower than the snow layer slowly emerge above it. In autumn, snow falling on refrozen pond ice blocks solar radiation from penetrating into the ponds and sea ice, thus reducing their radiation-effective area in August and September.

Because we are applying a climatological precipitation data set, we can not expect the effective area and depth of our melt ponds to behave exactly as observed. However, the modeled melt pond fractional area prior to snow radiative interference does exhibit some observed characteristics. For instance, Fig. 6 shows that the ponded fraction of ice near Barrow AK peaks within the first 2 weeks after forming, corresponding to Stages I and II of Polashenski et al. (2012): ponds form quickly and are widespread initially, particularly on level ice, then pool into low topographic features and begin to drain through permeable ice. Without macro channels as described by Polashenski et al. (2012), drainage is not as fast as observed. This model result could be improved by tuning the parameter d_p ; we consider its sensitivity later but leave detailed tuning for future work. Polashenski et al. (2012) state that in Stage III, pond coverage “increases steadily, often to its seasonal maximum” through changes in ice freeboard due to ice melting. While our simulated ponds do exhibit this second, slower maximum, it is associated more with continuing snow melt than adjustments in the sea ice freeboard. Sea ice topographic changes (due to ridging or ice melting completely) will cause the pond area to decrease in the model; only advection and the addition of melt water can increase simulated pond coverage. Neither flooding through permeable ice nor a water table residing in saturated sea ice below sea level (as modeled by Skjelkvåle et al., 2009) have been imple-

mented here. During Stage IV, the upper surfaces of ponds refreeze. As in the observations, this can (and does) occur at any time during the melt season, and snow on top of the pond ice increases the albedo.

Our simulations not only capture the essential characteristics of pond evolution, they also show a great deal of variability from year to year (Figs. 5 and 6), in spite of climatological precipitation and radiation forcing data. This behavior indicates that although the amount of precipitation is critical for pond volume and area, particularly in the spring and fall seasons, other physical variables that affect sea ice evolution contribute to interannual variations of melt pond processes. In the present runs, only air temperature,¹ humidity and the two wind components vary interannually, and therefore all variability seen here is due to the interaction of these four fields with sea ice feedback processes, particularly albedo.

Broadband albedo distributions are provided in Fig. 7, for comparison with Agarwal et al. (2011). The albedos presented here and in Agarwal et al. (2011) differ somewhat in how they are defined and accumulated or averaged. In particular, Agarwal et al. (2011) use retrievals taken daily at 1400 h, which have been normalized with respect to solar zenith angle and converted to a clear sky surface broadband albedo. Our model albedos include the effect of solar zenith angle in daily averages when the sun is above the horizon, and when it is below the horizon, albedo is not computed; these zero values are not included in the time averages. Lower zenith angles will tend to increase the mean albedo value because of its cosine dependence, especially for ponded ice (Briegleb and Light, 2007). Clouds will further increase the mean albedo value (Wiscombe and Warren, 1980). In the present configuration, a cloud cover climatology is applied for longwave radiation calculations, but for shortwave radiation, cloud effects are approximated via a partitioning of downwelling shortwave radiation into direct and diffuse components (Hunke and Lipscomb, 2010). In coupled configurations, an active atmospheric model component can supply computed direct and diffuse radiation components to the sea ice model for use in the radiation scheme. The present model employs a delta-Eddington approximation for multiple scattering (Briegleb and Light, 2007) radiative effects.

We find that the overall distributions of mid-month albedos resemble those of Agarwal et al. (2011), except that our simulations show a greater prevalence of high values associated with snow. In addition to the differences in definition noted above, this bias also reflects excess snow in the model. Furthermore,

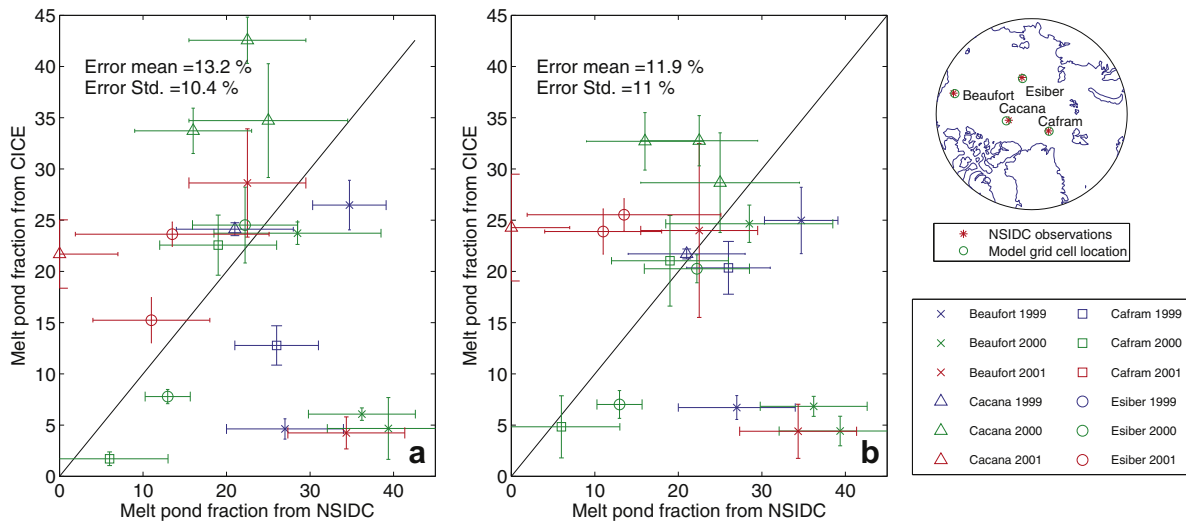


Fig. 9. Comparison of simulated and observed pond fraction for (a) CNTL (b) TALL. Observations are derived from high-resolution satellite imagery of four sites, in the Beaufort Sea, Canadian Arctic ('Cacana'), East Siberian Sea ('Esiber') and Fram Strait ('Cafram') (Fetterer et al., 2008). The mean value and standard deviation of the model error, compared with the observations, are given.

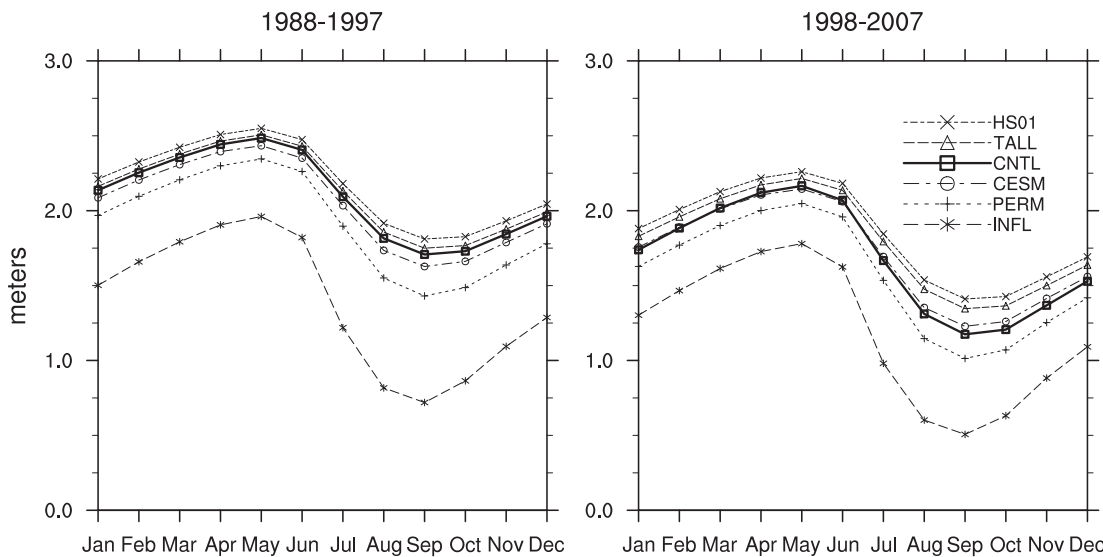


Fig. 10. Seasonal cycle of mean sea ice thickness for 1988–1997 and 1998–2007.

Wiscombe and Warren (1980) found that snow albedos are too high when calculated using a delta-Eddington approximation unless highly absorbing particles such as soot are included, particularly in visible wavelength bands (Warren and Wiscombe, 1980). Although aerosols have been included in one version of CICE (Holland et al., 2012), they are not active in the runs reported here. Therefore our snow albedos assume high values and contribute to the higher-than-observed ice areas evident in Fig. 1.

The strong peaks in April and May in Fig. 7 are associated with snow, and the distributions display the sharp decay toward higher values and long tail toward lower values seen in the observations. By June, the distribution has widened, with a primary peak at 0.7 (melting snow) and a secondary peak around 0.45, reflecting the influence of melt ponds; in Agarwal et al. (2011) this secondary peak appears at an albedo of approximately 0.55. The shift toward lower albedos continues in July, especially for ice in regions with smaller temporal coverage. In August and September the distribution shifts toward higher albedos as the ponds experience freeze-

up, and by mid-September the high-albedo snow peak is evident once again. As in the data, we can distinguish the different time thresholds in all months. Threshold years are chosen as in Agarwal et al. (2011), to which we have added the full 28-year distribution available from the model. Grid cells with sea ice of shorter duration tend to exhibit much lower albedo than those containing ice more often, reflecting a larger fraction of ocean albedo (0.06 here) as well as differing ice properties (thickness, age, snow cover) characteristic of these regions.

4.2. Sensitivities

We conduct a number of runs to test the sensitivity of the model to parameters in the melt pond scheme, as listed in Table 1.

Aspect ratio. The first of these runs tests the effect of our assumed shape for changes in pond volume, δ_p . In the control simulation, this parameter takes the value 0.8, following Holland et al. (2012) but the definition differs: in CESM, the entire pond volume

1998-2007

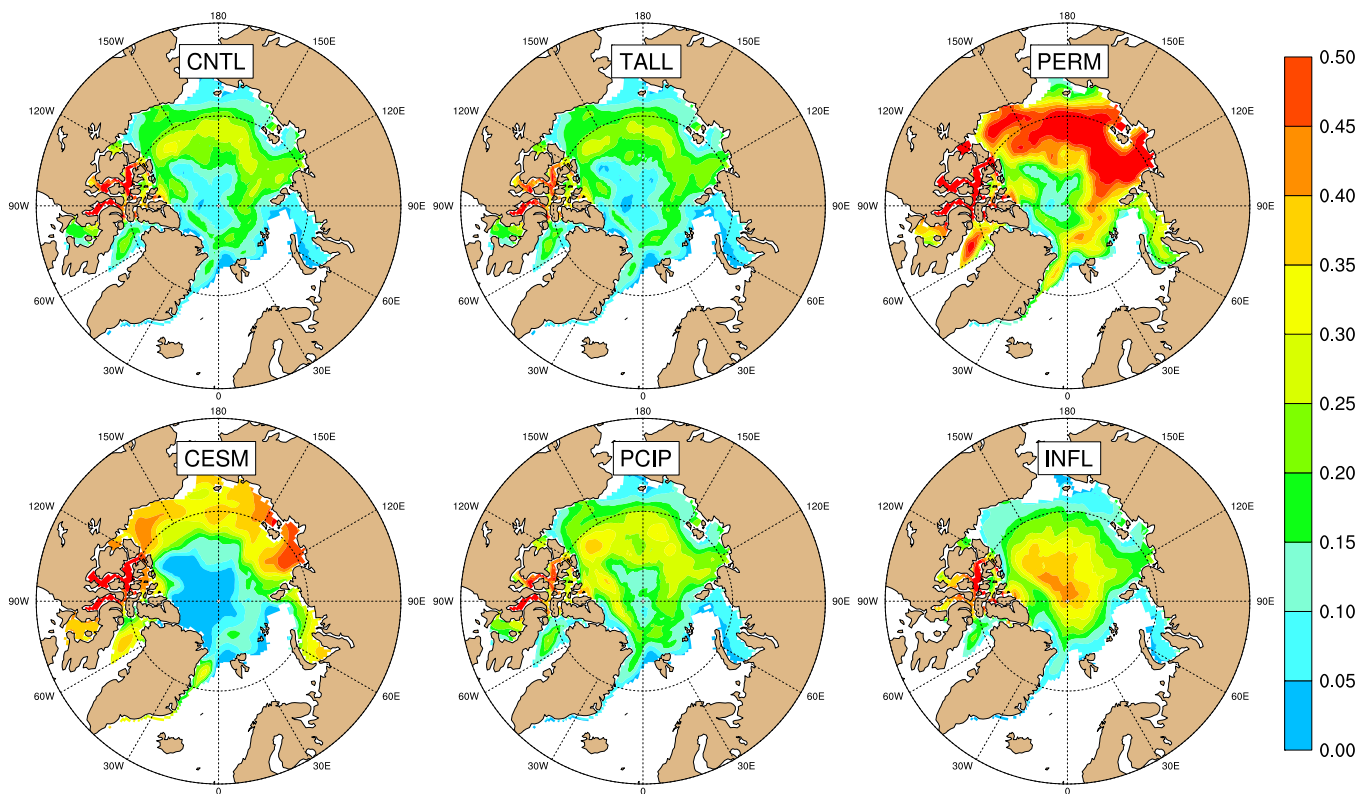


Fig. 11. July 1998–2007 mean effective pond area, as a fraction of ice area, for the control and five sensitivity simulations.

1998-2007

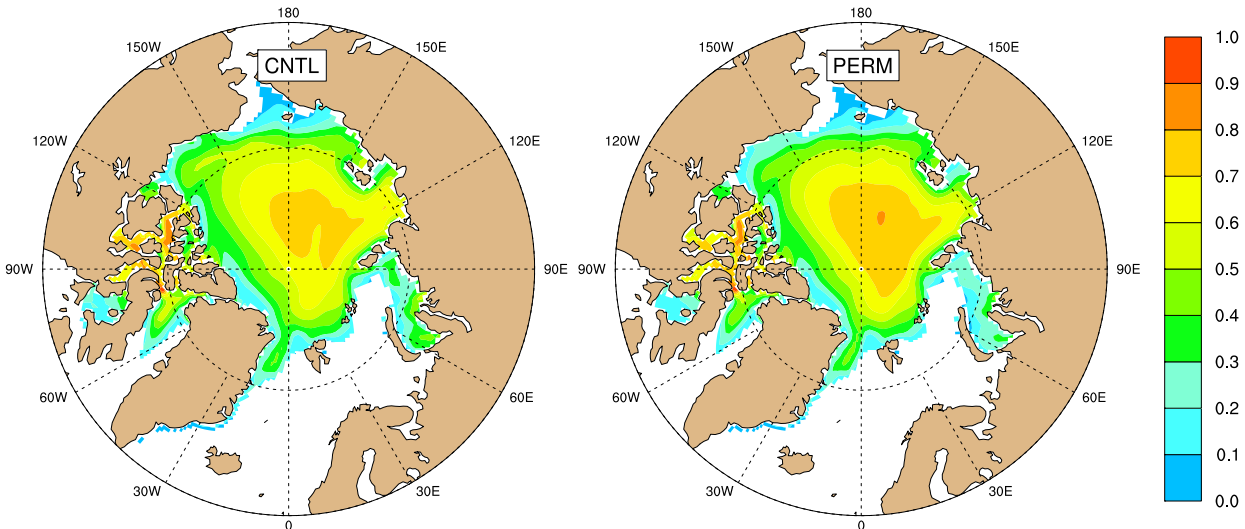


Fig. 12. Level ice fraction of ice area for CNTL and PERM.

V_p is initialized with this ratio of depth to area fraction at the beginning of each time step, and then other processes may alter it. In our runs, this ratio is used only for changes in pond volume, ΔV ; a shape is not imposed on existing pond volume. Thus, pond area and depth is more highly constrained in the CESM scheme than in the present melt pond parameterization, as seen in Fig. 8. Both schemes exhibit large area fractions and shallow depths early

in the melt season, with increasing depths relative to pond area through July. In August and September our ponds continue to deepen relative to pond area, while in CESM they start to become more shallow. This difference is associated with a mechanism imposed in CESM that limits pond depth to 90% of the ice thickness.

Fig. 8 also shows that in our parameterization the largest pond area coverage appears in June and July, while the deepest ponds

occur in July and August. Altering the shape of ΔV does not make a large difference to the simulations, although taller ponds ($\delta_p = 1.2$, TALL) achieve pond fractions slightly closer to observations at four Arctic sites that were monitored during 1999–2001 (Fetterer et al., 2008), as indicated in Fig. 9. Shallower ponds ($\delta_p = 0.4$, FLAT) cover more area and worsen the comparison. Altering the shape of ΔV does not make a significant difference to the total ice area and thickness in either case (compare CNTL and TALL in Fig. 10), because there is little change to the effective pond area (Fig. 11(a) and (b)), which is governed primarily by the infiltration scheme.

Initial runoff. Changing the parameter that controls the amount of meltwater allowed to run off of the ice, versus being accumulated in melt ponds, also creates only small differences in the simulations. Allowing less meltwater to run off (RFFDN) increases the pond volume and leads to slightly less ice and snow overall (not shown), even though in this test we are keeping *all* of the meltwater that would otherwise run off. Having a greater volume of pond water increases the drainage rate through permeable ice, somewhat compensating for the lack of initial runoff. Likewise, increasing the meltwater runoff (RFFUP) decreases the pond volume and leads to slightly more ice and snow. In both cases, there is less of a difference earlier in the season when the ice area fraction is close

to 1 and both cases have runoff close to 0. The change in both cases is small.

Permeability and the level ice response. By far, the strongest effects are achieved by turning entire processes off in the parameterization. For example, if the sea ice is made impermeable by setting $d_p = 0$ (PERM), then ponds can not drain through the ice and they cover a much larger area (Fig. 11). This effect is apparent especially on thinner ice that would tend to become more permeable and also is less ridged. This leads to thinner ice overall (Fig. 10), less snow and smaller sea ice concentrations, particularly in the summer.

Interestingly, the change in sea ice permeability also leads to more level ice, i.e., less ridging, as shown in Fig. 12. In the mechanical redistribution parameterization used in CICE, the redistribution of ice of a given thickness into a ridged ice thickness distribution depends on the thickness of the ice being ridged (Hunke, 2010, Fig. 1). If the deforming ice is thinner to begin with, then either the resulting deformed ice of a given thickness does not cover as large an area, or the newly ridged ice area has a smaller mean thickness, or both. The first case is consistent with the idea that at some point, the ice becomes so thick that it crumbles at the edges rather than piling up higher; thus thicker ice can make lower, broader ridges than thinner ice. In the second case, thinner

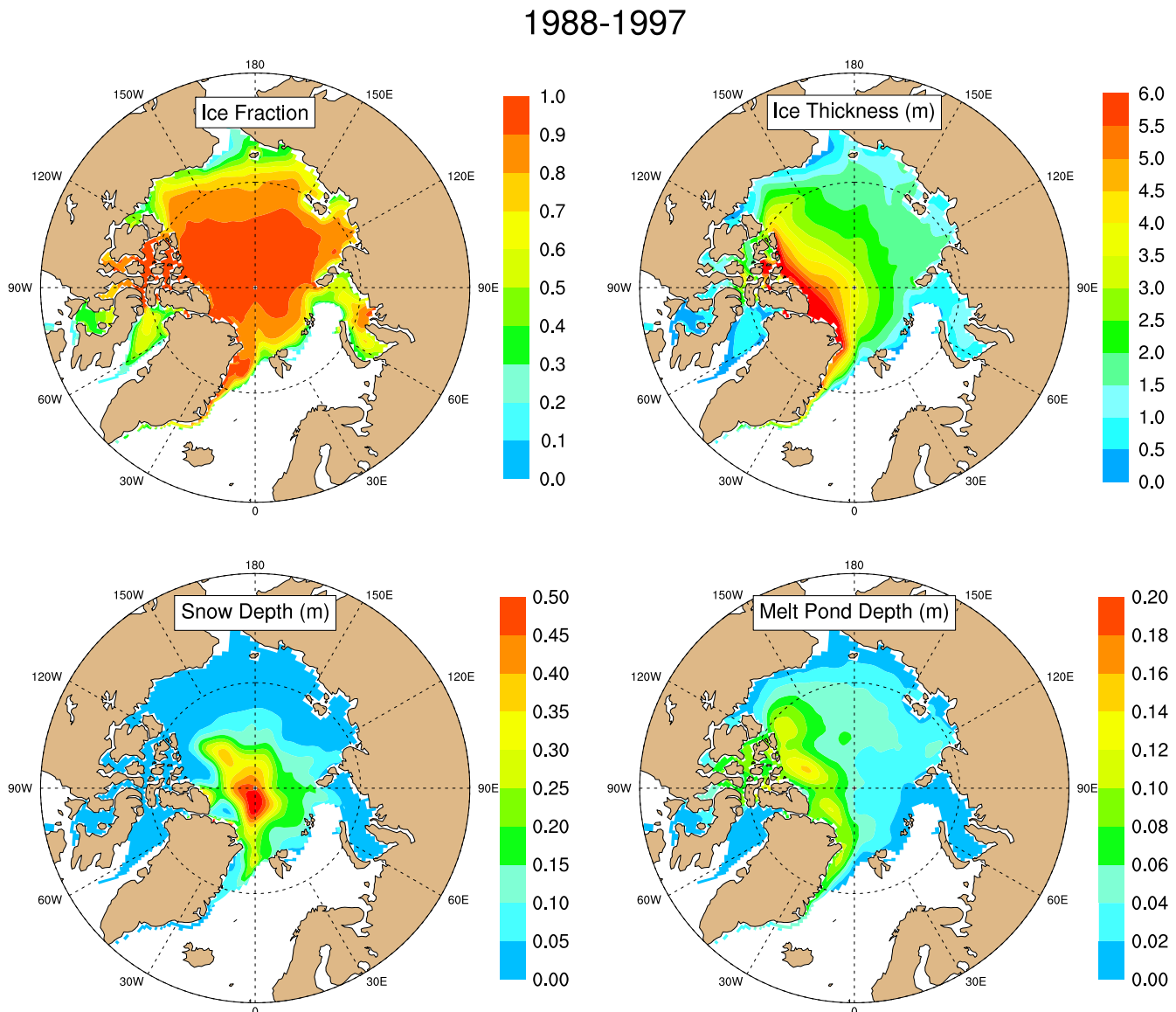


Fig. 13. July 1988–1997 mean ice area fraction, thickness, snow depth and pond depth from the control simulation, for comparison with Fig. 2.

undeformed ice does not pile up as much under the same convergent forcing field as thicker ice.

These simulations indicate a feedback in the level ice response that has not been described before, to our knowledge. Decreasing ice thickness leads to less ridged ice area, with more level ice remaining undeformed. This ice is thinner overall, which in turn leads to less ridging, more pond coverage, and a greater fraction of thinner ice. Note that unlike the ice–ocean albedo feedback, this process does not work as well in the other direction for thickening ice, because ridges stop thickening and the ice forms a rubble field when exceptionally thick (Hopkins, 1998).

Snow infiltration. Turning off snow infiltration processes (INFL) has the biggest effect of all these tests. Without hiding the ponds under the snow, the radiative effects of the ponds are much greater, the snow melts completely and the ice volume is much less (Fig. 10). The pond cycle shifts earlier, so that there is more pond area in June and less in August through October (not shown). Without snow present in July, the pond spatial pattern exhibits more ponds in the central Arctic (Fig. 11), and the level ice area increases for the same reason as in PERM.

Because the model is so sensitive to snow infiltration, we tested the snow saturation parameter, which determines when a pond begins to form from collecting melt water. Larger values of r_{sat} mean that more water is required to saturate the snow before ponds begin to form, and thus we ignore the radiative impact of the ponds for a longer period during the beginning of the melt season. With $r_{sat} = 0$ (RPO), the snow is assumed to be saturated at all times and ponds may become radiatively effective immediately. We also tested $r_{sat} = 0.3$ (RP03), and our tests indicate that this parameter makes very little difference to the simulation.

Snow density will affect the infiltration process, but extricating its effects on that process alone is difficult due to the many other

effects of snow density in the sea ice model, which is very sensitive to both ice and snow density (Kim et al., 2006). In this pond parameterization, we expect that making the snow less dense would cause the infiltrating ponds to appear later above the snow surface, thus decreasing their radiative effects and ultimately increasing snow and ice volume.

Snow also limits radiation reaching ponds that have a refrozen lid. Changing the patchy snow parameter h_{s1} from 0.03 m to 0.1 m (HS1) allows radiation to pass into the ponds for snow depths up to 10 cm, instead of blocking all radiation at 3 cm depths. The effective pond area, however, is quite similar to that in CNTL for most of the meltpond season because snow depths on the refrozen lids generally are small, and therefore the overall simulations are similar (not shown). Also, the transition from 0 to h_{s1} is linear, so that the largest potential differences in radiation arise for snow depths close to h_{s1} . Smaller values of h_{s1} will more effectively alter the radiation budget in the underlying ponds and sea ice by decreasing the snow depth at which all radiation is blocked. Thus, $h_{s1} = 0.01$ m leads to more snow, lower effective pond area, and thicker ice (Fig. 10), an effect amplified through an albedo feedback mechanism. Therefore h_{s1} could be considered a means for tuning the surface albedo. However, its usefulness is limited because very small values of h_{s1} cause the numerical model to fail to converge, due to sudden changes in incoming radiation when the snow melts completely (this is the primary reason for having this parameter), while larger values do not alter the results appreciably.

Interannually varying precipitation. For this test, we used the CORE interannual precipitation data for 1980–2007. In the hemispheric average over sea ice north of 60°N, the CORE precipitation for these years is approximately 0.08 cm/day less than the CORE “normal year” climatology used for the other simulations. Less snow on the ice in the variable precipitation case results in a larger

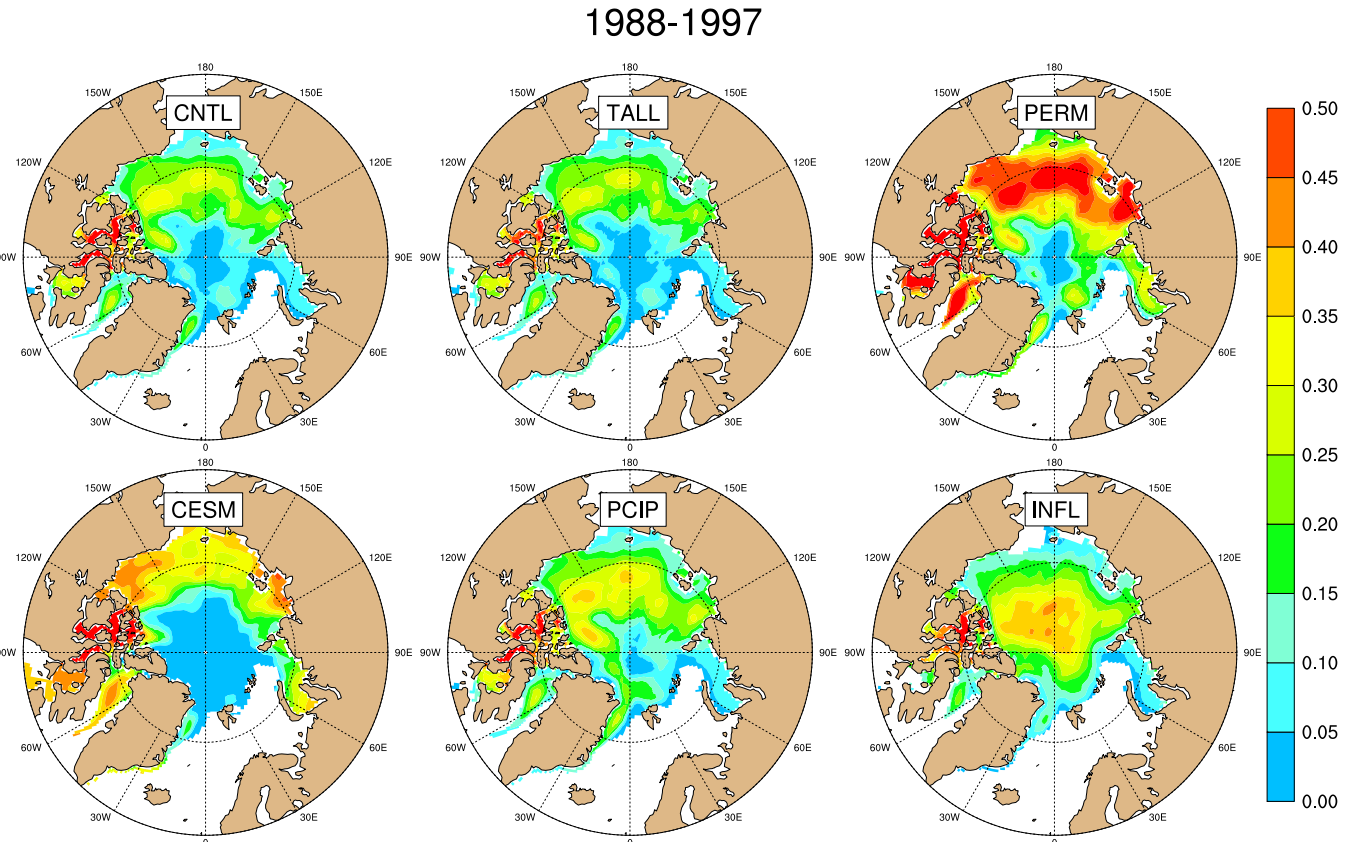


Fig. 14. July 1988–1997 mean effective pond area, as a fraction of ice area, for comparison with Fig. 11.

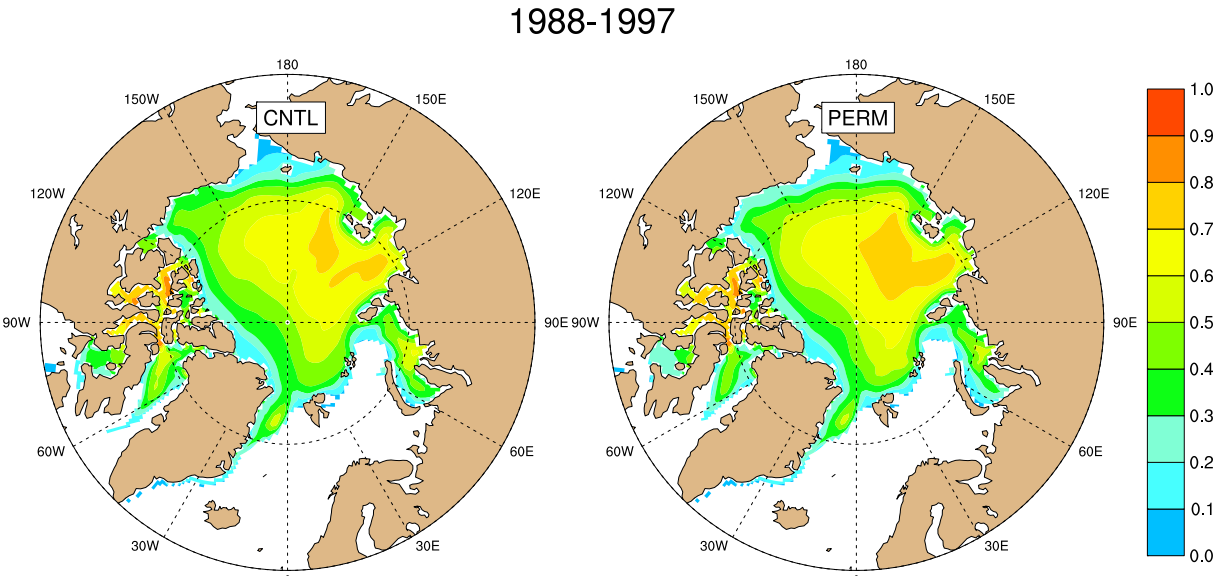


Fig. 15. Level ice fraction of ice area for CNTL and PERM, for comparison with Fig. 12.

effective pond area (Fig. 11) and thinner ice, but the sea ice concentration is essentially the same (not shown). Often, less snowfall in sea ice simulations results in thicker ice because the snow's insulating effect is reduced, allowing greater heat conduction and ice growth. In the present run, we suspect that this insulating effect is offset by increased radiation reaching the ice through ponds and melting it, such that we end up with slightly thinner ice than in the climatological precipitation run.

4.3. Interdecadal differences

Figs. 13 and 14 provide mean 1988–1997 fields for the control and sensitivity simulations discussed above, for comparison with 1998–2007 fields shown in Figs. 2 and 11. In all simulations we see that the ice fractional area, thickness and snow depth has decreased in the later decade, compared with the previous decade, while pond depth increased. Fig. 10 shows that the mean thickness over the Arctic decreased by about 0.3 m (slightly less in winter), in CNTL. Moreover, the maximum ice area shifts from April, on average in the decade 1988–1997, to March in 1998–2007, indicating a shorter sea ice growing season (not shown).

Snow melts more quickly in the later years, as is evident in Figs. 2 and 13, causing the maximum pond area to occur earlier (July in 1988–1997 and June in 1998–2007). Since the precipitation data is climatological for this case (CNTL), this difference is due to melting rates after the snow falls, including enhancement through albedo feedback. Comparing Fig. 14 with Fig. 11, it is clear that effective pond area in July 1998–2007 is larger in central areas (where the snowpack has not melted) for all runs except INFL. In this case, snow remaining on the sea ice does not affect the melt pond area radiatively; the effective pond area is smaller in the later decade because the ponds themselves are smaller, due to greater drainage rates. This case illustrates the delicate balance between precipitation amount, melt rates, pond volume, and snow infiltration processes in the model. Careful measurement of this balance in the physical system is needed to fully calibrate these subparameterizations.

Finally, Fig. 15 illustrates the level ice response in the model in the earlier years. The level ice area fraction increases as the ice thickness decreases in both CNTL and PERM, demonstrating that this feedback mechanism is active within each of these runs, in addition to being apparent in run comparisons. That is, as the ice

thins, the ridged ice area fraction decreases, leaving more level ice, which is thinner and can melt faster. Melt ponds can enhance this feedback because they spread out more on level ice than on ridged ice, thus increasing solar heating and further melting of the ice.

5. Discussion and conclusions

While an exhaustive comparison of this new meltpond scheme with the existing schemes of Holland et al. (2012) and Flocco et al. (2012) is beyond the scope of this paper, we can still comment on certain aspects of these parameterizations. For example, Fig. 10 shows that the sea ice thickness is similar in the CESM and CNTL runs. CESM ponds are much more extensive than CNTL during July and August, but in the central Arctic their effective area is less (Figs. 11 and 14), indicating that the mechanisms imposed on CESM melt ponds (shape, maximum pond depth dependent on ice thickness, shadowing melt ponds under more than 3 cm of snow) are more efficient at limiting pond radiative effects than the snow infiltration and pond drainage through permeable ice modeled in CNTL. Differences are magnified through the ice-albedo feedback, contributing to larger melt ponds in the CESM run. However, the exponential refreezing formula used for CESM is stronger than the Stefan growth condition used for CNTL (Eq. (7)), so that the effective pond area fraction in September is similar in the two runs. In spite of these significant differences in approach, the CESM and CNTL simulations of ice area and thickness are similar overall.

The primary difference between the present meltpond parameterization and that of Flocco et al. (2012) lies in how sea ice topography is taken into account when determining the areal coverage of ponds. Because Flocco et al. (2012) allow ponds to pool on the thinnest categories within a grid cell, draining melt water from thicker categories, their scheme is highly sensitive to changes in the thickness distribution discretization, particularly when increasing the number of categories. We expect our scheme to be less sensitive to the number of categories, although changes in the ice thickness distribution will have an impact because our meltpond parameterization depends closely on the simulation of deformed and level ice, which itself depends on the ice thickness distribution. We plan a thorough comparison of the level-ice and

Flocco et al. (2012) schemes, especially their dependence on modeled topography, for future investigation.

In this paper we have presented a parameterization of melt ponds carried as tracers on the simulated level ice area fraction. Physical descriptions of pond processes have been incorporated, including infiltration of melt water in snow, drainage through permeable ice, and pond refreezing. Snow in particular affects the radiative properties of the ponds, sometimes hiding them completely in both spring and fall. Melt ponds first appear at southerly latitudes in spring, moving north as the melt season progresses. Thinner ice tends to be more permeable than thicker ice, and therefore pond drainage is more evident on thinner ice. Because of variations in topography, we find deeper ponds on thicker, more deformed ice, and these are the last to freeze over in autumn. Ice on top of refrozen ponds can collect snow, thus preventing solar radiation from being absorbed below; this effect is most pronounced near the end of the summer but is present earlier in the season.

Our simulated melt ponds exhibit the four stages of pond evolution as outlined by Polashenski et al. (2012), following Eicken et al. (2002), although the increase of pond area in Stage III in the model is due to continuing snow and ice melt rather than direct connection with seawater through macroscopic flaws in the ice. Ponds deepen throughout the season, while their areal coverage first spikes then gradually increases until fall refreezing again shrinks them to nothing. Since the ponds are only radiatively effective in this implementation, the refrozen pond ice is not aggregated with the remaining sea ice in the fall; in a coupled system requiring mass and energy conservation, it would be treated the same way as the rest of the melt water (i.e., passed to the ocean).

Except when entire subprocesses are omitted, our simulations are not highly sensitive to most parameters in the meltpond scheme, with the exception of the parameter that controls when ponds are visible underneath snow on refrozen pond ice (h_{s1}). Processes associated with the snow (e.g., infiltration, precipitation) are most important for the meltpond simulation because they control the timing of the pond seasonal cycle, and therefore the mass balance of the sea ice. With the exception of INFL, the spatial patterns of sea ice area, thickness, snow and pond characteristics are similar across all simulations, including the CESM test using an entirely different meltpond parameterization. Sea ice thickness (and thus volume) varies among the runs, but its spatial distribution does not except near the ice edge, where ice may be missing in some runs and very thin in others.

Although they utilize a great deal of climatological forcing, the CICE simulations presented here resemble reality. Ice area and thickness both decrease in time, with more substantial losses in ice volume during the last decade of the run. Interannual variability is significant throughout the simulations, driven by the four non-climatological forcing fields: air temperature, humidity and the two components of wind velocity. Feedback processes are important for strengthening the variability. Although it was not discussed here, the model incorporates a thermodynamic (slab) ocean mixed layer, and the computed effect of ice–ocean albedo feedback on sea surface temperature is critical. Other feedback processes also contribute, including the ice-albedo feedback (changing ice surface characteristics enhance or reduce melting) and a level-ice-pond mechanism in which thinning ice has more level surface area available to be covered in ponds, enhancing thinning.

We also identified compensating effects that tend to maintain the sea ice status quo. First, with less snow insulating the ice (in the more recent decade), we would expect greater conduction and sea ice growth in winter, but increased radiation penetrating the ice slows growth and/or enhances summer melting. The second compensating effect applies to meltponds: increased melting

should increase pond volume, but greater permeability in warmer, melting ice allows greater pond drainage.

The complexity of sea ice surface processes, and melt ponds in particular, require detailed measurements to unravel. At the same time, basin-wide observations of melt pond characteristics are needed for evaluation of large-scale modeling techniques such as ours. We commend those researchers involved in this in situ and remote sensing fieldwork, which is now yielding the wealth of enlightening observations necessary for detailed model development.

Acknowledgments

This modeling venture originated as a student project during the 2011 IARC Summer School on “Modeling of the Arctic Climate System,” held at the International Arctic Research Center in Fairbanks, Alaska, in May 2011. We extend special thanks to John Walsh and Vladimir Alexeev for organizing this event. Hunke is supported by the Earth System Modeling and Regional and Global Climate Modeling programs of the Office of Biological and Environmental Research within the U.S. Department of Energy’s Office of Science; Los Alamos National Laboratory is operated by the National Nuclear Security Administration of the DOE under Contract No. DE-AC52-06NA25396. D. Hebert is supported by NRL’s 6.1 Core Program “Determining the Impact of Sea Ice Thickness on the Arctic’s Naturally Changing Environment (DISTANCE)” (Program Element PE 0602435N). O. Lecomte is partly supported by the European Commission’s 7th Framework Programme, under Grant Agreement No. 226520, COMBINE Project (Comprehensive Modelling of the Earth System for Better Climate Prediction and Projection).

References

- Agarwal, S., Moon, W., Wettlaufer, J.S., 2011. Decadal to seasonal variability of arctic sea ice albedo. *Geophys. Res. Lett.* 38, L20504. <http://dx.doi.org/10.1029/2011GL049109>.
- Assur, A., 1958. Composition of sea ice and its tensile strength. In: Arctic Sea Ice; Conference held at Easton, Maryland, February 24–27, 1958. Publs. Natl. Res. Coun. Wash. Washington, DC, US 598, 106–138.
- Bitz, C.M., Lipscomb, W.H., 1999. An energy-conserving thermodynamic sea ice model for climate study. *J. Geophys. Res. – Oceans* 104, 15669–15677.
- Briegleb, B.P., Light, B., 2007. A Delta-Eddington multiple scattering parameterization for solar radiation in the sea ice component of the Community Climate System Model. NCAR Tech. Note NCAR/TN-472-STR, National Center for Atmospheric Research.
- Cavalieri, D., Parkinson, C., Gloersen, P., Zwally, H.J., 1996, updated 2008. Sea ice concentrations from Nimbus-7 SMMR and DMSP SSM/I passive microwave data, 1979–2008. National Snow and Ice Data Center, Boulder, Colorado USA, digital media.
- Collins, W.D., Bitz, C.M., Blackmon, M.L., Bonan, G.B., Bretherton, C.S., Carton, J.A., Chang, P., Doney, S.C., Hack, J.J., Henderson, T.B., Kiehl, J.T., Large, W.G., McKenna, D.S., Santer, B.D., Smith, R.D., 2006. The community climate system model version 3 (CCSM3). *J. Clim.* 19, 2122–2143.
- Curry, J.A., Schramm, J.L., Ebert, E.E., 1995. Sea ice-albedo climate feedback mechanism. *J. Clim.* 8, 240–247.
- Eicken, H., Grenfell, T.C., Perovich, D.K., Richter-Menge, J.A., Frey, K., 2004. Hydraulic controls of summer Arctic pack ice albedo. *J. Geophys. Res.* 109, C08007. <http://dx.doi.org/10.1029/2003JC001989>.
- Eicken, H., Krouse, H.R., Kadko, D., Perovich, D.K., 2002. Tracer studies of pathways and rates of meltwater transport through arctic summer sea ice. *J. Geophys. Res.* 107, 8046. <http://dx.doi.org/10.1029/2000JC000583>.
- Fetterer, F., Wilds, S., Sloan, J., 2008. Arctic sea ice melt pond statistics and maps, 1999–2001. National Snow and Ice Data Center, Boulder, CO, digital media.
- Flocco, D., Feltham, D.L., 2007. A continuum model of melt pond evolution on Arctic sea ice. *J. Geophys. Res.* 112, C08016. <http://dx.doi.org/10.1029/2006JC003836>.
- Flocco, D., Feltham, D.L., Turner, A.K., 2010. Incorporation of a physically based melt pond scheme into the sea ice component of a climate model. *J. Geophys. Res.* 115, C08012. <http://dx.doi.org/10.1029/2009JC005568>.
- Flocco, D., Schroeder, D., Feltham, D.L., Hunke, E.C., 2012. Impact of melt ponds on arctic sea ice simulations from 1990 to 2007. *J. Geophys. Res.*, in press, <http://dx.doi.org/10.1029/2012JC008195>.
- Gent, P.R., Danabasoglu, G., Donner, L.J., Holland, M.M., Hunke, E.C., Jayne, S.R., Lawrence, D.M., Neale, R.B., Rasch, P.J., Vertenstein, M., Worley, P.H., Yang, Z.-L., Zhang, M., 2011. The community climate system model version 4. *J. Clim.* 24, 4973–4991.

- Grenfell, T.C., Perovich, D.K., 2004. Seasonal and spatial evolution of albedo in a snow–ice–land–ocean environment. *J. Geophys. Res.* 109. <http://dx.doi.org/10.1029/2003JC001866>.
- Griffies, S.M., Biastoch, A., Böning, C., Bryan, F., Danabasoglu, G., Chassignet, E.P., England, M.H., Gerdes, R., Haak, H., Hallberg, R.W., Hazeleger, W., Jungclaus, J., Large, W.G., Madec, G., Pirani, A., Samuels, B.L., Scheinert, M., Gupta, A.S., Severijns, C.A., Simmons, H.L., Tregier, A.M., Winton, M., Yeager, S., Yin, J., 2009. Coordinated ocean–ice reference experiments (COREs). *Ocean Mod.* 26, 1–46.
- Holland, M.M., Bailey, D.A., Briegleb, B.P., Light, B., Hunke, E., 2012. Improved sea ice shortwave radiation physics in CCSM4: the impact of melt ponds and aerosols on arctic sea ice. *J. Clim.* 25, 1413–1430.
- Hopkins, M.A., 1998. Four stages of pressure ridging. *J. Geophys. Res.* 103, 21883–21891.
- Hunke, E., Holland, M., 2007. Global atmospheric forcing data for Arctic ice–ocean modeling. *J. Geophys. Res.* 112, C06S14. <http://dx.doi.org/10.1029/2006JC003640>.
- Hunke, E.C., 2001. The elastic–viscous–plastic sea ice dynamics model: a review. In: Dempsey, J.P., Shen, H.H. (Eds.), *Scaling Laws in Ice Mechanics and Ice Dynamics, Solid Mechanics and Its Applications*, vol. 94. Kluwer, pp. 289–299.
- Hunke, E.C., 2010. Thickness sensitivities in the CICE sea ice model. *Ocean Mod.* 34, 137–149. <http://dx.doi.org/10.1016/j.ocemod.2010.05.004>.
- Hunke, E.C., Dukowicz, J.K., 1997. An elastic–viscous–plastic model for sea ice dynamics. *J. Phys. Oceanogr.* 27, 1849–1867.
- Hunke, E.C., Dukowicz, J.K., 2002. The elastic–viscous–plastic sea ice dynamics model in general orthogonal curvilinear coordinates on a sphere – effect of metric terms. *Mon. Wea. Rev.* 130, 1848–1865.
- Hunke, E.C., Lipscomb, W.H., 2010. CICE: the Los Alamos Sea Ice Model, Documentation and Software User's Manual, version 4.1. Tech. Rep. LA-CC-06-012, Los Alamos National Laboratory, Los Alamos, New Mexico. <<http://climate.lanl.gov/Models/CICE>>.
- Jordan, R., Albert, M., Brun, E., 2008. Physical processes within the snow cover and their parameterization. In: *Snow and Climate: Physical Processes, Surface Energy Exchange and Modeling*, p. 12.
- Kim, J.G., Hunke, E.C., Lipscomb, W.H., 2006. A sensitivity analysis and parameter tuning scheme for global sea-ice modeling. *Ocean Mod.* 14, 61–80.
- Lipscomb, W.H., Hunke, E.C., 2004. Modeling sea ice transport using incremental remapping. *Mon. Wea. Rev.* 132, 1341–1354.
- Lüthje, M., Feltham, D.L., Taylor, P.D., Worster, M.G., 2006. Modeling the summertime evolution of sea-ice melt ponds. *J. Geophys. Res.* 111, C02001. <http://dx.doi.org/10.1029/2004JC002818>.
- Notz, D., 2005. Thermodynamic and fluid-dynamical processes in sea ice. Ph.D. thesis, University of Cambridge, UK.
- Perovich, D.K., Grenfell, T.C., Light, B., Hobbs, P.V., 2002a. Seasonal evolution of the albedo of multiyear Arctic sea ice. *J. Geophys. Res.* 107, 8044. <http://dx.doi.org/10.1029/2000JC000438>.
- Perovich, D.K., Grenfell, T.C., Richter-Menge, J.A., Light, B., Tucker III, W.B., Eicken, H., 2003. Thin and thinner: Sea ice mass balance measurements during SHEBA. *J. Geophys. Res.* 108, 8050. <http://dx.doi.org/10.1029/2001JC001079>.
- Perovich, D.K., Tucker, W.B., Ligett, K.A., 2002b. Aerial observations of the evolution of ice surface conditions during summer. *J. Geophys. Res.* 107, 8048. <http://dx.doi.org/10.1029/2000JC000449>.
- Polashenski, C., Perovich, D.K., Courville, Z., 2012. The mechanisms of sea ice melt pond formation and evolution. *J. Geophys. Res.* 117, C01001. <http://dx.doi.org/10.1029/2011JC007231>.
- Pringle, D.J., Eicken, H., Trodahl, H.J., Backstrom, L.G.E., 2007. Thermal conductivity of landfast Antarctic and Arctic sea ice. *J. Geophys. Res.* 112, C04017. <http://dx.doi.org/10.1029/2006JC003641>.
- Rösel, A., Kaleschke, L., Birnbaum, G., 2012. Melt ponds on arctic sea ice determined from MODIS satellite data using an artificial neural network. *The Cryosphere* 6, 431–446.
- Rothrock, D.A., 1975. The energetics of the plastic deformation of pack ice by ridging. *J. Geophys. Res.* 80, 4514–4519.
- Scott, F., Feltham, D.L., 2010. A model of the three-dimensional evolution of arctic melt ponds on first-year and multiyear sea ice. *J. Geophys. Res.* 115, C12019. <http://dx.doi.org/10.1029/2009JC005363>.
- Skyllingstad, E.D., Paulson, C.A., Perovich, D.K., 2009. Simulation of melt pond evolution on level ice. *J. Geophys. Res.* 114, C12019. <http://dx.doi.org/10.1029/2009JC005363>.
- Sturm, M., Massom, R., 2010. Snow and sea ice. In: Thomas, D.N., Dieckmann, G.S. (Eds.), *Sea Ice*, second ed. Wiley-Blackwell, pp. 153–204.
- Taylor, P.D., Feltham, D.L., 2004. A model of melt pond evolution on sea ice. *J. Geophys. Res.* 109, C12007. <http://dx.doi.org/10.1029/2004JC002361>.
- Thorndike, A.S., Rothrock, D.A., Maykut, G.A., Colony, R., 1975. The thickness distribution of sea ice. *J. Geophys. Res.* 80, 4501–4513.
- Warren, S.G., Wiscombe, W.J., 1980. A model for the spectral albedo of snow II: snow containing atmospheric aerosols.. *J. Atmos. Sci.* 37, 2734–2745.
- Wiscombe, W.J., Warren, S.G., 1980. A model for the spectral albedo of snow I: pure snow. *J. Atmos. Sci.* 37, 2712–2733.